

3.N21/5:6/2989

GOVT. DOC.

NACA IN 2787

NATIONAL ADVISORY COMMITTEE FOR AERONAUTICS

TECHNICAL D. PT.
BUSINESS AND

Aug 15 '53

TECHNICAL NOTE 2989

COMPARISON OF SECONDARY FLOWS AND BOUNDARY-LAYER
ACCUMULATIONS IN SEVERAL TURBINE NOZZLES

By Milton G. Kofskey, Hubert W. Allen, and Howard Z. Herzig

Lewis Flight Propulsion Laboratory
Cleveland, Ohio



Washington
August 1953

NATIONAL ADVISORY COMMITTEE FOR AERONAUTICS

TECHNICAL NOTE 2989

COMPARISON OF SECONDARY FLOWS AND BOUNDARY-LAYER ACCUMULATIONS
IN SEVERAL TURBINE NOZZLES

By Milton G. Kofskey, Hubert W. Allen, and Howard Z. Herzig

SUMMARY

An investigation of secondary-flow loss cores originating in turbine nozzle blade passages was conducted by means of flow visualization studies and detailed flow measurements. The degree to which blade surface velocity profiles affect the magnitude and concentration of loss cores was investigated by comparing three nozzle blade configurations.

For all cases, high loss values were measured in the fluid downstream of the corners formed by the suction surfaces of the blades and the shrouds; and these losses were accompanied by discharge angle deviations from design values.

Flow visualization studies and flow measurements at the lower Mach numbers indicate that when, as a result of unfavorable blade surface velocity profiles, thickened blade boundary layers exist on the blades near the outer shroud, they may provide the conditions required for passage vortex formation. Under these conditions sizable outer shroud loss cores are found at the nozzle discharges. Blades having thinner two-dimensional profile boundary layers, however, appear to offer resistance to passage vortex formation near the outer shroud, and instead there results inward radial flow of low momentum air in the blade wake. Under these conditions the inner shroud loss region at the nozzle discharge is large, while the outer shroud loss region may, in comparison, be quite small.

In both cases reduced loss accumulations along the outer shroud are obtained at the higher Mach number as shock-boundary-layer thickening on the blade surface provides an additional path for the radially inward flow of low momentum fluid. The results therefore indicate that passage-vortex formation may not exist for all blade configurations and flow conditions and may be governed, to a large extent, by blade boundary-layer thickness and separation.

Comparison of well-designed constant-discharge-angle and free-vortex type blades indicates that the secondary-flow loss differences for these blades were so small that the choice of the type of blading, based solely on secondary flows, is of negligible concern.

INTRODUCTION

Secondary flows in turbomachines give rise to relatively large regions of low-energy fluids, causing flow blockages and deviations from design flow angles to which are attributed reduced efficiency and performance ratings. The increasing severity of the effects of secondary flows on losses as velocity and mass flow per unit frontal area in turbomachines have increased has given added impetus to the study of secondary-flow behavior in turbomachines. Various analytical methods have been developed (refs. 1 to 4) to evaluate and predict the deviations in exit flow angles and velocities due to the secondary flows in channels.

More recent investigations at the NACA Lewis laboratory (refs. 5 to 7) have concentrated on obtaining experimentally an over-all picture of the actual secondary flows. Reference 5 shows the development of the so-called passage vortices in the end-wall boundary layers of nozzle cascades. Reference 6 gives information concerning the effects of the radial pressure gradients on the secondary-flow components, and reference 7 isolates and evaluates these components in a typical turbine nozzle annular cascade. As a result of the complicated three-dimensional patterns of the secondary flows established in references 5 to 7, considerable doubt exists whether a physically valid analytical description of secondary flows in turbine nozzle cascades can be presently obtained by use of such simplifying assumptions as two-dimensional flows, no viscosity in the turning fluid, or nontwisting Bernoulli surfaces which are typical of assumptions currently used for theoretical analyses.

Accordingly, the present investigation of secondary flow is part of an experimental program conducted at the NACA Lewis laboratory using the methods which were successfully adapted in references 5 to 7, that is, flow visualization and detailed flow measurements. In particular, the blade section surface velocity profile, which may be a contributing factor to secondary-flow loss cores, is considered. The degree to which this affects the magnitude and concentration of the loss cores is investigated by comparing three nozzle blade configurations: a cascade of constant-discharge-angle blades designed for smooth blade section velocity profiles; a cascade of constant-discharge-angle blades having irregular blade section velocity profiles with velocity peaks, conducive to boundary-layer separation, over a large part of the blade span (particularly near the blade tip); and a cascade of free-vortex design blades having smooth blade section velocity profiles. For the experimental investigation, detailed pressure and flow angle data were taken

in free-stream, wake, and boundary-layer regions at the nozzle discharge. These tests were conducted at high subsonic and at supersonic hub discharge Mach numbers. Flow visualization studies were made along the blade surfaces and shrouds by means of hydrogen sulfide and paint traces and by smoke flow tests as described in reference 5.

APPARATUS AND PROCEDURE

Test Unit

A schematic view of the test unit used in this investigation is shown in figure 1. A filter was installed in a large depression tank (not shown in fig. 1) upstream of the test section to prevent damage and clogging of the delicate instruments by dirt particles from the air supply. The filter consisted of two layers of 1/4-inch felt separated by filter paper supported by wire mesh screening. A second depression tank downstream of the first tank was located approximately 4 duct diameters (approximately 6 ft) upstream of the nozzle blades (fig. 1). A long-radius nozzle was installed in the depression tank to provide smooth entry into the duct leading to the nozzle blades in the test section. A fine mesh screen was also installed in the tank to give a uniform inlet velocity distribution. The air discharged from the nozzle blades into an annular duct having six straightening vanes located approximately 3 tip diameters downstream of the nozzle blades.

Turbine Nozzle Blades

For purposes of simplicity, the three blade configurations investigated will be designated as follows: blade A, a constant-discharge-angle blade with smooth surface velocity profile designed by the stream-filament method; blade B, a constant-discharge-angle blade with a more blunt leading edge and a more irregular surface velocity distribution, particularly near the blade tip; and blade C, a smooth-velocity-profile, stream-filament design having free-vortex velocity distribution. The suction surface velocity profiles at the hub, mean, and tip sections of the three blades are presented in figure 2. Mean section blade shapes are shown in figure 2(b).

All nozzle blades used in the investigation were of subsonic design for an equivalent weight flow of approximately 15.3 pounds of air per second. The 48 blades for each set have a hub-to-tip radius ratio of 0.730 and a tip diameter of 16.25 inches. Blades A and C were designed by the two-dimensional stream filament method described in reference 8. As the stream-filament method applies only to the portion of the blades forming the channel, the blades were designed to do the greatest amount of the turning within the channel. The trailing-edge portion of the

blade having little curvature was faired at the approximate discharge angle. Blade profile and stacking coordinates for the three blade sets are given in tables I to III.

Constant-discharge-angle blades (blade A). - These blades were designed for a constant discharge angle of 56° from axial. The blade chord and trailing-edge thickness vary from respective values of 1.642 and 0.049 inch at the tip to 1.173 and 0.034 inch at the hub. The blades have a solidity of 1.510 at the hub and 1.545 at the tip.

Constant-discharge-angle blades (blade B). - These blades, from a production turbine, were designed for a constant discharge angle of approximately 60° from axial and have a solidity of 1.489 at the hub and 1.497 at the tip. The chord and trailing-edge thickness vary from respective values of 1.592 and 0.040 inch at the tip to 1.157 and 0.026 inch at the hub.

Vortex-type blades (blade C). - The blades were designed for a free-vortex-type velocity distribution with a discharge angle of approximately 65° from axial at the hub. The blades have a solidity of 1.507 at the hub and 1.595 at the tip. The chord and trailing-edge thickness vary from respective values of 1.696 and 0.044 inch at the tip to 1.172 and 0.034 inch at the hub.

Instrumentation

The instrumentation of the cascade and the locations of the measuring stations are described in detail in reference 6. The instruments used to obtain the detailed flow surveys are shown in figure 3 of reference 6.

Experimental Procedure

In general, the flow measurements and flow visualization studies of blades B and A were made in a manner similar to that employed with blade C. These methods are reported in reference 6. At the time of the investigation of blade B, which was conducted first, the techniques required for boundary-layer and surface flow studies had not yet been developed; therefore these studies were not made for blade B.

Flow conditions. - The reference inlet total pressure was held constant at approximately 26.50 inches of mercury absolute and the inlet total temperature, at 553° R for all surveys. Each of the three sets of blades was investigated at two hub discharge Mach numbers as follows: blade A, 0.86 and 1.36; blade B, 1.18 and 1.41; blade C, 0.94 and 1.46. Smoke studies of flow direction were made on blades A and B at very low air velocities.

Flow-measuring surveys. - The pressure surveys for blades A, B, and C were made as described in reference 6.

The use of the double-tube pressure probe for boundary-layer flow-angle surveys was developed near the end of the investigation of blade C in reference 6. In the present investigation of blade A, a comparison was made of the free-stream angles measured by the double-wire hot-wire anemometer probe and the double-tube pressure probe. Differences in measured angles were found to be 1° or less over most of the passage. The greatest difference, approximately 2° , occurred near the shrouds where the rates of radial variation in discharge angle are large. Because of its small size the double-tube pressure probe is considered more reliable than the double-wire hot-wire anemometer probe in regions where the rate of radial variation in discharge angle is high. Because of this and because of its greater simplicity in operation, all angle data in the free stream and in the boundary layers (for blade A) were taken with the double-tube pressure probe. No flow angle measurements were made at positions less than 0.1 inch from the shrouds for blade B.

Surface flow-direction studies. - Visual studies of the flow direction along the blade and wall surfaces for blades A and C were made in two ways (ref. 5). The first technique used the reaction between white lead carbonate painted on the surface and hydrogen sulfide gas which was admitted through an appropriately located wall static tap and mixed with the boundary-layer air flowing through the cascade. The resulting darkening of the lead carbonate showed the direction of flow along the surface from the static tap. The hydrogen sulfide gas pressure was adjusted to exceed the static pressure at the tap by only enough (0.02 in. Hg, approximately) to cause it to flow into the passage without blowing it away from the surface and without upsetting local flow conditions. The second technique involved softening the lead carbonate with glycerin until it would flow slightly along the surface because of viscous effects between air and paint. A comparison of results obtained by these two techniques showed good agreement; hence, patterns on the surface were considered to indicate air-flow direction and the results were recorded photographically.

Smoke flow-direction studies. - Smoke studies of flow direction using the technique of reference 5 were made with blade types A and B mounted in the annular cascade (fig. 1). The airspeed through the cascade was held to a maximum of about 20 feet per second in order to avoid diffusion of the smoke and keep the smoke sufficiently concentrated for photographing. The smoke was introduced into the air stream just upstream of the blades at two radial positions for each blade, namely, adjacent to the outer shroud and near midsection. Photographs were made of the resulting flow patterns at the blade discharge.

Calculation Procedures

Loss calculations. - Results of total-pressure and static-pressure-tap data are presented as contours of kinetic energy loss, which is defined as follows:

$$\text{Loss} = 1 - \eta = 1 - \frac{v^2}{v_1^2} = \frac{\left(\frac{p}{P}\right)^{\frac{\gamma-1}{\gamma}} - \left(\frac{p}{P_1}\right)^{\frac{\gamma-1}{\gamma}}}{1 - \left(\frac{p}{P_1}\right)^{\frac{\gamma-1}{\gamma}}}$$

The symbols are defined in the appendix.

Mass averaging. - Discharge angles, velocities, and loss were mass averaged by the following expression:

$$\frac{\int x \rho V_a \, d\theta}{\int \rho V_a \, d\theta}$$

The use of weighted averages, where possible, in preference to ordinary arithmetic averages is discussed in reference 9.

Circulation. - Circulation was determined by the following equation:

$$\Gamma = V_\theta r$$

This equation was adapted for use in this investigation from a similar equation developed in reference 10, pp. 62 ff.

RESULTS

Results presented include kinetic energy loss distributions and discharge angle distributions for the flow investigations of three blade configurations. Also presented are comparisons of circulation distributions and results of hydrogen sulfide and paint traces and of smoke flow studies.

Loss Distribution

Inlet surveys. - Inlet surveys of total and static pressure and flow angle were practically identical for all three blade configurations.

Figure 3 shows the inlet loss obtained from such surveys for blade A. Static pressure and flow angle were practically constant over the annulus, and losses in total pressure occurred only in the shroud boundary layers. The combination of constant total pressure, constant static pressure, and constant flow angle produced an inlet velocity distribution which was considered satisfactory.

Discharge loss for blade A. - Negligible losses were observed for blade A over most of the flow passage (figs. 4(a) and 4(b)). The major losses were found in the shroud boundary layers, the blade wakes, and particularly in the vicinity of the corners formed by blade suction surfaces and shrouds. The measured blade wake loss values were small compared with those in the shroud boundary layers and the other loss regions. For the loss regions outside the shroud boundary layers (that is, more than approximately 0.040 in. from the shrouds), loss areas and magnitudes were such as to indicate a reduction in loss near the outer shroud with increasing Mach number and an increase in loss near the inner shroud with increasing Mach number. This result is also shown in the curves of loss plotted against radial position (fig. 5) where the value at each radial position is obtained by mass-averaging the loss across one passage width at that radius.

Comparison of discharge losses (blades A and C). - No significant difference in magnitude is noted between losses for blades A and C (figs. 4(a), 4(b), 4(e), and 4(f)). For each blade the size of the loss region and the over-all magnitude of the losses decreased at the outer shroud with increasing Mach number while increasing at the inner shroud. In both cases the extents of the measured wakes decreased with increasing Mach number (for blade A at the higher Mach number, the wake loss dropped below the 5 percent contour to a minimum of 3.5 percent), but the losses distributed throughout the passage (regions marked 1 on the contour plots) increased with increasing Mach number. This is also apparent in the mass-average plots (figs. 6(a) and 6(b)) where the values are affected not only by losses in the boundary layers, loss regions, and wakes but also by losses distributed throughout the passage.

Comparison of discharge losses (blades A, B, and C). - Figures 4(c) and 4(d) show loss contours for blade B. Comparison with the contours for blades A and C (figs. 4(a), 4(b), 4(e), and 4(f)) shows significant differences. At both Mach numbers the wake loss is small for blade B, being less than 5 percent through almost the entire wake length for the lower Mach number. The outer shroud loss region for blade B at the lower Mach number is greater in magnitude and extent than and different in shape from those regions for the other two blades; and although it diminishes with increasing Mach number as for the other blades, it is still appreciable at the higher Mach number. The inner shroud loss region outside the shroud boundary layer increases with increasing Mach number for blade B as for the other two blades, but for blade B it

becomes much larger, with maximum loss at the higher Mach number of 67 percent to compare with 21 percent for blade A and 25 percent for blade C.

Some of the results indicated by the contour plots also appear on the mass average loss plots (fig. 6). The decrease of loss at the outer shroud and increase at the inner shroud with increasing Mach number is apparent on the mass-average plots. Also, the difference in flow behavior between blade B and the other two blades shows up as differences between their wake losses, between losses near inner shrouds, and between losses near outer shrouds.

Discharge Angle Distribution

Discharge angles for blade A. - The results of the discharge angle surveys for blade A are shown as contours in figures 7(a) and 7(b). Angle gradients for the lower Mach number were negligible over most of the passage. However, they were greater for the higher Mach number. The variation in discharge angle across the passage at a radial distance of 0.1 inch from the inner shroud was found to increase from 4.1° for the lower Mach number to 8.9° for the higher Mach number. In each case the greatest variation in discharge angle outside the boundary layers occurred in the large loss regions typically found near the inner shroud in all nozzle configurations.

In figure 8 the circumferentially mass-average discharge angle computed for blade A is plotted against radius for each of the two Mach numbers. The computed angles show that in the central part of the passage the turning had approximate design value, but that as either shroud was approached there appeared a decrease in discharge angle relative to design value. Near the inner shroud this decrease was more pronounced for the higher Mach number than for the lower Mach number. The reverse was true for the decrease near the outer shroud. Also, at points nearer the shrouds, the discharge angle increased, showing overturning in the boundary layers at the measuring station.

Comparison of discharge angle distributions. - Contour plots of discharge angles (figs. 7(a), 7(b), 7(c), 7(d), 7(e), and 7(f)) and radial plots of mass-average discharge angles (figs. 9(a) and 9(b)) show good agreement at the lower Mach numbers over most of the passage between design angle and measured angle for blades A and C and fair agreement for blade B. At these lower Mach numbers the only severe angle gradients were in the boundary layers. At the higher Mach numbers, the contour plots show the effects of considerable disturbance in the direction of discharge flow distributed through the passage for all three blades, although blades A and C show mass-average values which are still near design values over most of the passage. Blade B at the higher Mach

number shows severe angle gradients in the inner shroud loss region, with underturning amounting to as much as 22° and overturning of about 8° . At a radial distance of 0.1 inch from the inner shroud, the circumferential variations in measured discharge angles were 4.1° , 2.4° , and 2.6° for blades A, B, and C, respectively, at the lower Mach numbers. At the higher Mach numbers the corresponding variations were 8.9° , 25.0° , and 9.5° , respectively.

For blades A and C, as either shroud was approached (figs. 9(a) and 9(b)), there appeared decreases in mass-average discharge angle relative to design value. Near the inner shroud a decrease appeared for blade B also. The decreases near the inner shroud were more pronounced at the higher Mach number, whereas near the outer shroud the decreases were smaller for the higher Mach number. Also, in the shroud boundary layers themselves, the discharge angle increased, showing overturning in the boundary layers.

Circulation Distributions

Adjusted design and measured spanwise variations in mass-average circulation are shown in figure 10 for the three sets of blades at the two Mach numbers. As design and measured Mach numbers are approximately the same at the lower Mach number run for blade C, design and actual spanwise circulation can be compared directly. For the other cases, design and actual Mach numbers are different, and the design circulation in each case was therefore adjusted in magnitude to provide agreement with the measured values while maintaining the correct ratio between outer shroud and inner shroud circulation for that design. This was done to emphasize any variations in experimentally determined spanwise circulation resulting from secondary-flow effects.

The variations of mass-average circulation obtained from measurements are seen to be in good agreement with the adjusted design variations through the greater part of the passage. However, in the boundary layers of blades A and C where the discharge angle measurements are available and indicate considerable overturning, the experimental circulation increased as the shroud was approached. This continued to the point where the velocity in the boundary layer became small enough to overbalance the effect of discharge angle increase. At this point the circulation began to decrease rapidly. In loss regions, also, experimental values of circulation were affected by the low velocities and the high discharge angle gradients. An extreme example of this appears in figure 10(b) for blade B, where the experimentally obtained mass-average circulation decreases from its midspan value approximately 20 percent as the inner shroud is approached.

Figure 10 shows that the design spanwise distribution of circulation is not greatly different for the two types of blade design, vortex and constant discharge angle.

Surface Flow Traces

Figures 11 and 12 present hydrogen sulfide and paint traces which show the same secondary-flow phenomena for blade A as those reported earlier (refs. 6 and 7) for blade C. Figure 11(a) shows an upstream view of hydrogen sulfide traces on the inner shroud indicating the cross-channel path of the gas from its origin in static taps near the leading edges of the blades. Similar traces were formed on the outer shroud by hydrogen sulfide gas emitted from outer shroud static taps. Figure 11(b) shows the same traces, in a view from downstream, as the low momentum air accumulated on the suction surfaces near the trailing edges of the blades.

Figure 11(c) for the lower Mach number and figure 12 for the higher Mach number present results which indicate, for blade A, radial flows of the types discussed in references 6 and 7. In figure 11(c) blade 1 is painted at the tip on the pressure surface, blades 2 and 3 at midspan on the suction and pressure surfaces, respectively, and blades 4 and 5 at the root on suction and pressure surfaces, respectively. For each blade the paint is shown to have flowed around to the trailing edge and inward along the trailing edge to the hub, indicating the probable existence of radial flow at the trailing edge for the lower Mach number. Figure 12 shows paint traces for the higher Mach number indicating radial flow inward along the trailing edge and also along the suction surface of the blade through the boundary layer where it was thickened by encountering a shock across the passage from the trailing edge of the adjacent blade. Blades 1 and 2 in figure 12 had their entire suction surfaces painted, and these blades show not only the flow path inward along the suction surfaces but also hydrogen sulfide traces where the low momentum air flowed out or accumulated on the suction surfaces near the trailing edges. Blades 3 and 4 were painted near the outer shroud on their suction and pressure surfaces, respectively. Blade 3 shows the suction surface flow path and blade 4 shows flow down the trailing edge and around to the suction surface near the root. Blades 5 and 6 were painted at midspan on their suction and pressure surfaces, respectively, and present paint traces showing probable radial flow behind the trailing edge and in the thickened portion of the suction surface boundary layer.

Smoke Flow-Direction Studies

The sole purpose of the smoke flow-direction studies was to indicate any basic differences which may exist in boundary layer and

secondary-flow behavior between the two blade configurations A and B. When smoke was introduced to the flow passage in such a manner that it would enter the outer shroud boundary layer and follow the motion of the low momentum air through the passage, it was found that the flow paths were different for the two constant-discharge-angle blade configurations, blade A and blade B. Presumably, such differences were due to the same blade characteristics which produced different surface velocity profiles for the blades. For blade B (fig. 13), the smoke was observed to flow against the suction surface at the outer shroud and, as it approached the blade trailing edge, it divided, most of it rapidly sweeping on downstream near the shroud and the remainder turning sharply to follow the trailing edge. When the introduction of smoke was suddenly interrupted, that which had followed the trailing edge clung to the blade surface, eddied mildly, slowly merged with the through-flow air, and gradually disappeared. The slowness of this motion indicated that, although the picture shows a large accumulation of smoke, the fraction of outer shroud low momentum fluid taking this radial flow path was small.

For blade A (fig. 14(a)) the behavior was different in that no such eddying in a large stagnant region was found. Instead, while the smoke showed a rapid radial flow component, it also had a rapid through-flow component on the suction surface so that it was largely swept out into the wake at points somewhat removed from the outer shroud.

The smoke similarly showed this difference between the flow behavior of the two blades when it was introduced about midway between the shrouds (figs. 13(b) and 14(b)).

DISCUSSION

Loss Distributions

As a result of secondary flow (cf. ref. 7, Introduction), the low momentum air in the shroud boundary layers tends to move across the passage in the direction from the pressure surface toward the suction surface and to accumulate in the corners between shroud and suction surface. This is indicated by the hydrogen sulfide traces of figures 11 and 12 and the loss contour plots of figure 4.

Radial pressure gradients also exist in an annular cascade of nozzle blades and will drive low momentum fluid radially to the inner shroud wherever a region of low through-flow velocity provides a complete path. The paint traces of figures 11(c) and 12, for example, show indications of such paths. At the lower Mach number in figure 11(c) the paint has been swept in along the trailing edge of the blade. At the higher Mach number in figure 12 an additional path is indicated on the suction surface of the blade near the trailing edge.

Loss distributions, blades A and C. - The loss contours for blade C which were discussed thoroughly in references 6 and 7 are similar to the loss contours for blade A to a noteworthy degree. Accordingly, the following discussion of the loss contours obtained with blade A can be considered equally applicable to blade C.

Loss contours (fig. 4(a)) at the lower Mach number for blade A indicate an outer shroud loss region which is distributed over a portion of the wake in such a way as to suggest that, at the measuring plane, radial pressure gradients had forced its movement toward the inner shroud, but that its through-flow component of velocity was such as to prevent a large part from actually reaching the inner shroud. Indications of the same kind of boundary-layer flow behavior at low flow Mach numbers are seen in the photographs in figure 14.

The inner shroud loss region under these conditions is composed of inner shroud boundary-layer air with the addition of some low momentum air reaching it by radial flow from the blade surface boundary layer, and the measured wake is a combination of profile loss with some low momentum air reaching it by radial flow from points nearer the outer shroud.

At the higher Mach number the flow is different, mostly because of the additional path for radial flow provided by shock-boundary-layer thickening on the blade suction surface (fig. 12). This seems to allow the greater part of the outer shroud loss region to reach the inner shroud and combine with inner shroud losses to form the large region of low momentum fluid which was measured and appears in figure 4(b).

The mass-average loss curves (fig. 5) indicate a greater loss throughout the mainstream for the higher Mach number than for the lower Mach number, even though the contour plots show that the wake is smaller. Reference to the original data gives the reason for this. At the higher Mach number the loss distributed through the passage outside the wake is appreciable (about 1 percent in order of magnitude), whereas it is negligible at the lower Mach number. This leads one to suspect that at the higher Mach number a mild general flow disturbance exists in the exit air from the passage. Because a comparison of blades A and C indicates that secondary flow differences are small, it appears that the choice of type blading, based solely on secondary flows, is of negligible concern.

Loss distributions, blade B. - As noted in the RESULTS section, the loss contours for blade B (figs. 4(c) and 4(d)) are considerably different from the loss contours for blades A and C (figs. 4(a), 4(b), 4(e), and 4(f)). Not only the large size but also the regular shape of the loss region near the outer shroud downstream of nozzle blade B at the lower Mach number (fig. 4(c)) is noteworthy. The symmetric high

loss region closely surrounded by regions of considerably lower loss indicates qualitatively the existence of a core of low momentum fluid, possibly a flow vortex.

The combination of large outer shroud loss core, comparatively small wake, and comparatively small inner shroud loss core at the lower Mach number indicates relatively little radial flow for blade B at these conditions. However, at the higher Mach number for blade B, the existence of considerable radial flow is indicated by the large inner shroud loss region and the reduction of the outer shroud loss core (fig. 4(d)).

Discharge Angle Distributions

For all three blades at the lower Mach numbers, the gradients of deviation of the discharge angles from design are quite small over most of the flow passage (figs. 7(a), 7(c), 7(e), and 9(a)). Furthermore, the circumferential mass-average flow angles (fig. 9(a)) are close to the design angles except near the shrouds.

For the higher Mach numbers (figs. 7(b), 7(d), 7(f), and 9(b)), however, discharge angle gradients distributed in the main stream are increased. This effect is expected if, as suggested in a previous section, there is an increasing general flow disturbance throughout the entire passage with increasing Mach number. As noted in the RESULTS section, the decreases in mass-average flow angles relative to design values were more pronounced near the inner shroud at the higher Mach numbers, whereas near the outer shroud the decreases were smaller for the higher Mach numbers. This is attributed to a combination of Prandtl-Meyer type expansion off the blade trailing edge (amounting to 5° at a Mach number of 1.25) and increased accumulation of low momentum fluid near the inner shroud which effectively blocked the flow and induced an increase in axial velocities in the immediate vicinity. Underturning and overturning of this magnitude result in rotor blade angles of attack which would cause a noticeable deterioration in performance. In this connection it is noted that for blade C (ref. 6) a nozzle discharge angle variation of 13.6° near the inner shroud led to a variation in rotor blade angle of attack of 16.9° and a resulting loss of 1.5 percent of energy based on tangential component of velocity.

Large angle gradients were found in the shroud boundary layers, also, where overturning appears due to cross-channel, secondary flows.

Correlation of Results on Three Blade Configurations

Results obtained from the investigation of the three turbine nozzle blade types show how the different accumulations of loss, the different

wake phenomena, and the different visual indications of secondary flow may possibly be correlated with each other and with the blade shapes and velocity profiles. For example, in figure 4(c) the presence of a sizable loss core (suggestive of a flow vortex) for the lower Mach number near the outer shroud downstream of nozzle blade B is noted. By comparison, figures 4(a) and 4(e) present the loss contours for the lower Mach numbers for blades A and C in which such large outer shroud loss cores do not appear. It is clear that the secondary flows which result in two such different loss distribution patterns must themselves be considerably different. The reasons for these differences are discussed qualitatively in this section. The discussion falls into three main parts.

First, suction surface velocity profiles are discussed and differences are noted in the boundary layer near the tip of blade B as compared with the other blade types. The discussion then considers the probable effects of these boundary-layer differences upon the behavior of the cross-channel secondary flows at the outer shrouds. Finally, these considerations are shown to account for the differences in extent and magnitude of the wake losses measured behind the different kinds of blades and to provide an insight into the physical significance of such wake measurements.

Velocity profiles. - Suction surface velocity profiles are plotted together for the three blades for hub, mean, and tip sections in figures 2(a), 2(b), and 2(c), respectively. Mean section blade shapes are also shown in figure 2(b). The profiles were computed in each case for design (subsonic) Mach number. At other Mach numbers (at least in subsonic cases) velocity maximums and minimums might be expected to appear in similar locations.

For blades A and C, the profile plots show no sharp velocity peaks over the surface at any section. The blade B profile at the hub section, while not so smooth as the profiles of blades A and C, has only one maximum and might be expected to produce a fairly smooth type of flow. However, at the mean and particularly at the tip sections, blade B has profiles with two and three maximums, respectively, and each peak indicates a sudden change in velocity at one point. This nonuniformity may be actually greater than indicated because the calculation methods based on differential procedures and on representation of flow functions at a fixed number of points have a tendency to smooth the curves and thereby reduce the magnitude of all velocity peaks computed. Such irregular profiles might reasonably be expected to cause a difference in boundary-layer behavior between blade B and the other two blades by causing flow separation or unusual boundary-layer growth.

Boundary layers. - The effects of blade shape and velocity profile on blade surface boundary layer as described were shown visually by the smoke injection studies. Figure 13 for blade B indicates the presence

of a large separated region on the suction surface of the blade where the tip section velocity profile could be expected to affect the boundary layer. Apparently, the flow path followed by the smoke and accompanying low momentum air did not actually reach the inner shroud in the vicinity of the trailing edge.

For blade A, having a smooth velocity profile, figure 14(a) shows flow behavior which indicates that the boundary layer on the blade suction surface was thinner than for blade B and was not separated.

Vortex formation. - The difference between blade suction surface boundary layers previously indicated may be a basis for the difference between the large outer shroud loss region found with blade B and the much smaller outer shroud loss regions found with the other two blades. For blade B, the separated flow near the outer shroud provided the condition required for formation of an appreciable vortex. That is, the outer shroud boundary-layer air flowing into such a region might, and for blade B apparently did, roll up into the passage vortex type of flow described in reference 5. Once formed, the vortex resisted turning (ref. 5) and tended to maintain its direction of flow and passed into the wake near the outer shroud where measurements showed the presence of a sizable loss core.

At the higher Mach number for blade B, the additional radial flow path provided by the thickened boundary layer on the blade suction surface due to shock formation in the passage serves to drain off more of the low momentum fluid toward the inner shroud. This action effectively reduces the magnitude of the roll-up into a passage vortex.

No evidence of appreciable passage vortex formation near the outer shroud was observed for blades A and C for which the blade boundary layers are thinner, as has been pointed out. The greatest portion of the low momentum fluid originating along the outer shroud was swept radially inward into the wake and therefore was a contributing factor for the increased wake losses as compared with blade B. Also, for blades A and C, the part of the low momentum fluid reaching the inner shroud contributes to the greater size of the inner shroud loss region as compared with that at the outer shroud.

Thus, the results suggest that passage vortex formation of measurable magnitude may not take place under all secondary flow conditions but only in those cases where blade shape and velocity profiles are such as to cause development of boundary-layer separation and stagnation regions extensive enough for the purpose.

Wake losses. - The phenomena described indicate an inward radial transfer of a smaller fraction of low momentum fluid from the outer shroud to the inner shroud for blade B than for the other blades. Thus,

a smaller amount of low momentum fluid from the outer shroud was found in the wake for this blade than for the others, as shown on the contour plots in figure 4. The magnitude and extent of wake loss found behind a blade may, in some measure, be an indication of the radial flow taking place at the trailing edge or on the blade suction surface. Substantiating evidence is also indicated by the results of a study on blade C at the higher Mach number (ref. 7, figs. 3(b) and 12(a)) in which a flow fence was used to interrupt these radial flows. With the radial flow from the upper half of blade C interrupted at midspan, the loss measured in the wake from the lower half of the blade was reduced considerably.

At the lower Mach number, the loss accumulation for blade B near the inner shroud has roughly the same magnitude as for the other two blades. However, for blade B, with little radial flow, the greatest percentage of this loss must originate from the inner shroud boundary layer. For the other blades the measured inner shroud loss region is a combination of inner shroud loss and loss transferred radially in the wakes from the outer shroud. Barring radial flow, therefore, blades A and C would have smaller inner shroud loss regions to compare with that of blade B.

Circulation. - The differences between the types of spanwise circulation distributions for the three types of blades were shown to be small. Furthermore, the total variations in circulation over the major portions of the blade spans are small compared with the changes in circulation in the blade-end boundary-layer regions. These circumstances make it difficult to judge, from the investigations of these blades, how spanwise variation in circulation affects secondary flow patterns and loss distribution.

SUMMARY OF RESULTS AND CONCLUSIONS

The following results and conclusions were obtained from a study of secondary flows and loss accumulations in annular cascades of turbine nozzle blades of three different designs:

1. Two blade configurations (constant-discharge-angle blade A and vortex blade C, both with smooth suction surface velocity profiles) showed the same secondary-flow patterns, namely, cross-passage boundary-layer flow on the shrouds from pressure surfaces to suction surfaces and radial flow inward along the trailing edges of the blades. In addition, at supersonic conditions radial flow took place inward along the suction surface through a strip of the boundary layer which had been thickened by shock interaction. These effects result in a pronounced accumulation of low momentum air near the inner shroud and a greatly reduced outer shroud loss region.

2. For these two blade configurations (blades A and C), measured loss magnitudes and distributions were approximately the same and no extreme discharge angle gradients were encountered in the measuring plane.

3. Comparison of the two sets of blades having smooth velocity profiles (types A and C) with a set (constant discharge angle) which had irregular suction surface velocity profiles (type B) shows that losses in general were greatest and most concentrated for the blade with poorest velocity profiles. For this blade configuration, blade B, a passage vortex was apparently formed which carried a large loss region downstream near the outer shroud. At the higher Mach number this blade configuration showed indications of radial flow of large amounts of low momentum fluid to form a large loss region near the inner shroud, accompanied by severe discharge angle gradients.

4. The blade flow conditions which contribute to formation of a passage vortex near the outer shroud appear to be blade boundary-layer thickening and separation which are produced by irregular suction surface velocity profiles.

5. Magnitude and extent of blade wakes is dependent upon secondary flow conditions. The loss measured in the wake at any radial position is a combination of profile losses and low momentum air flowing inward from points nearer the outer shroud. Thus, the blade configuration having little tendency for passage vortex formation has, as a result, more pronounced wakes.

6. Because of the similarity between loss magnitudes and distributions and between secondary flows for the two blade configurations having smooth velocity profiles (constant-discharge-angle blade A and vortex blade C), it appears that on this basis alone there is no reason to choose one of the two blade types rather than the other. The difference between design spanwise circulation variation for the two is small, and the large boundary-layer and secondary flow effects seem to mask any effects which may exist because of the main span circulation differences.

Lewis Flight Propulsion Laboratory
National Advisory Committee for Aeronautics
Cleveland, Ohio, April 30, 1953

APPENDIX - SYMBOLS

The following symbols are used in this report:

$d\theta$	infinitesimal increment in circumferential distance
M_H	hub discharge Mach number
P	local total pressure, in. Hg
P_1	reference inlet total pressure, in. Hg
p	local static pressure, in. Hg
r	radius measured from axis, ft
V	local velocity, ft/sec
V_a	local axial component of velocity, ft/sec
V_i	ideal velocity as determined by reference inlet total pressure and local discharge static pressure, ft/sec
V_θ	local tangential component of velocity, ft/sec
x	local measured value, variable used in mass-averaging expression
Γ	circulation, sq ft/sec
γ	ratio of specific heats
η	local blade efficiency, V^2/V_i^2
ρ	static density, slugs/cu ft

REFERENCES

1. Carter, A. D. S., and Cohen, Elizabeth M.: Preliminary Investigation into the Three-Dimensional Flow Through a Cascade of Aerofoils. R. & M. No. 2339, British A.R.C., Feb. 1946.
2. Squire, H. B., and Winter, K. G.: The Secondary Flow in a Cascade of Airfoils in a Nonuniform Stream. Jour. Aero. Sci., vol. 18, no. 4, Apr. 1951, pp. 271-277.
3. Hawthorne, William R.: Secondary Circulation in Fluid Flow. Gas Turbine Lab., M.I.T., May 1950.
4. Kronauer, Richard E.: Secondary Flows in Fluid Dynamics. Pratt and Whitney Res. Rep. No. 132, Gordon McKay Lab., Harvard Univ., Apr. 1951.
5. Hansen, Arthur G., Herzig, Howard Z., and Costello, George R.: A Visualization Study of Secondary Flows in Cascades. NACA TN 2947, 1953.
6. Allen, Hubert W., Kofskey, Milton G., and Chamness, Richard E.: Experimental Investigation of Loss in an Annular Cascade of Turbine Nozzle Blades of Free Vortex Design. NACA TN 2871, 1953.
7. Rohlik, Harold E., Allen, Hubert W., and Herzig, Howard Z.: Study of Secondary-Flow Patterns in an Annular Cascade of Turbine Nozzle Blades with Vortex Design. NACA TN 2909, 1953.
8. Huppert, M. C., and MacGregor, Charles: Comparison Between Predicted and Observed Performance of Gas-Turbine Stator Blade Designed for Free-Vortex Flow. NACA TN 1810, 1949.
9. Scarborough, James B.: Numerical Mathematical Analysis. The Johns Hopkins Press (Baltimore), 1947.
10. Zucrow, Maurice Joseph: Principles of Jet Propulsion and Gas Turbines. John Wiley & Sons, Inc., 1948.

TABLE I. - NOZZLE BLADE PROFILE COORDINATES FOR BLADE A

(a) Profile coordinates.



X, in.	Section					
	Root		Mean		Tip	
	Radius, in.					
	5.939		7.003		8.122	
	Y _L , in.	Y _U , in.	Y _L , in.	Y _U , in.	Y _L , in.	Y _U , in.
0	0.036	0.036	0.046	0.046	0.050	0.050
.100	.025	.183	.022	.197	.021	.213
.200	.064	.232	.067	.258	.069	.280
.300	.090	.250	.099	.285	.104	.318
.400	.105	.246	.119	.292	.131	.131
.500	.110	.229	.131	.283	.149	.335
.600	.105	.206	.133	.266	.158	.324
.700	.093	.177	.126	.242	.157	.304
.800	.077	.146	.115	.213	.151	.280
.900	.058	.115	.101	.185	.140	.254
1.000	.036	.084	.083	.156	.127	.227
1.100	.013	.053	.064	.127	.111	.198
1.173	.017	.017	----	----	----	----
1.200	----	----	.042	.098	.093	.170
1.300	----	----	.020	.069	.073	.142
1.409	----	----	.022	.022	----	----
1.500	----	----	----	----	.029	.084
1.600	----	----	----	----	.004	.055
1.642	----	----	----	----	.025	.025

TABLE I. - NOZZLE BLADE PROFILE COORDINATES FOR BLADE A - Concluded



(b) Stacking coordinates.

X, in.	Section		
	Root Y, in.	Mean Y, in.	Tip Y, in.
0.071	0.073	-----	-----
.100	-----	0.102	-----
.128	-----	-----	0.131
.385	.175	-----	-----
.414	-----	.205	-----
.442	-----	-----	.234
.675	.140	-----	-----
.705	-----	.170	-----
.733	-----	-----	.199

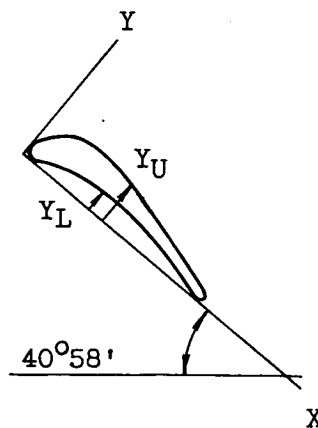


TABLE II. - NOZZLE BLADE PROFILE COORDINATES FOR BLADE B

(a) Profile coordinates.



X, in.	Section					
	Root		Mean		Tip	
	Radius, in.					
	5.939		7.003		8.122	
	Y_L , in.	Y_U , in.	Y_L , in.	Y_U , in.	Y_L , in.	Y_U , in.
0	0.083	0.083	0.099	0.099	0.117	0.117
.125	.001	.248	.004	.279	.000	.304
.225	.052	.286	.045	.327	.037	.361
.325	.079	.297	.080	.347	.076	.393
.425	.096	.291	.102	.351	.106	.406
.525	.104	.275	.115	.342	.124	.403
.625	.105	.249	.121	.325	.133	.392
.725	.099	.216	.121	.300	.138	.376
.825	.085	.177	.114	.268	.138	.351
.925	.063	.133	.101	.231	.131	.321
1.025	.035	.086	.081	.189	.118	.286
1.125	.005	.038	.059	.144	.100	.247
1.157	.013	.013	----	----	----	----
1.225	----	----	.035	.100	.081	.204
1.325	----	----	.009	.052	.058	.158
1.373	----	----	.017	.017	----	----
1.425	----	----	----	----	.035	.114
1.525	----	----	----	----	.011	.065
1.592	----	----	----	----	.020	.020

TABLE II. - NOZZLE BLADE PROFILE COORDINATES FOR BLADE B - Concluded

(b) Stacking coordinates.



X, in.	Section		
	Root Y, in.	Mean Y, in.	Tip Y, in.
0.206	0.167	-----	-----
.325	-----	0.210	-----
.385	.175	-----	-----
.446	-----	-----	0.252
.505	-----	.218	-----
.625	-----	-----	.260
.706	.143	-----	-----
.826	-----	.180	-----
.946	-----	-----	.208

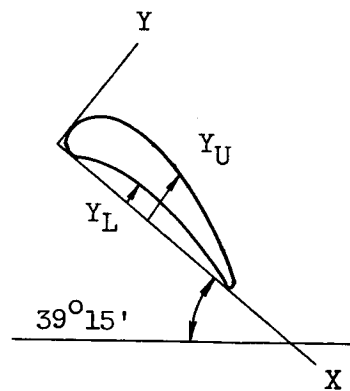



TABLE III. - NOZZLE BLADE PROFILE COORDINATES FOR BLADE C

(a) Profile coordinates.



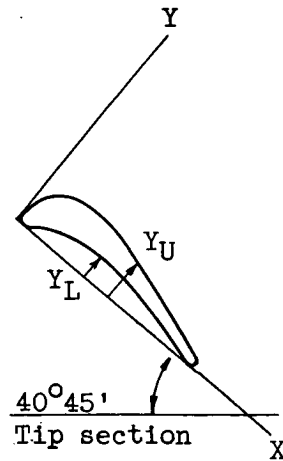
X, in.	Section					
	Root		Mean		Tip	
	Radius, in.					
	5.939		7.003		8.122	
	Y _L , in.	Y _U , in.	Y _L , in.	Y _U , in.	Y _L , in.	Y _U , in.
0	0.038	0.038	0.059	0.059	0.082	0.082
0.100	.032	.183	.016	.216	.002	.238
.200	.089	.237	.071	.267	.047	.292
.300	.130	.264	.109	.292	.087	.320
.400	.153	.268	.134	.300	.117	.311
.500	.160	.257	.147	.293	.138	.329
.600	.154	.234	.152	.279	.151	.319
.700	.139	.206	.149	.259	.159	.303
.800	.116	.174	.140	.235	.159	.283
.900	.087	.138	.124	.207	.153	.260
1.000	.055	.099	.104	.177	.142	.234
1.100	.020	.058	.082	.145	.127	.207
1.172	.017	.017	----	----	----	----
1.200	----	----	.056	.112	.109	.180
1.300	----	----	.030	.079	.089	.152
1.400	----	----	.001	.044	.067	.123
1.428	----	----	.020	.020	----	----
1.500	----	----	----	----	.043	.095
1.600	----	----	----	----	.019	.067
1.697	----	----	----	----	.022	.022

TABLE III. - NOZZLE BLADE PROFILE COORDINATES FOR BLADE C - Concluded



(b) Stacking coordinates.

X, in.	Section		
	Root	Mean	Tip
	Y, in.	Y, in.	Y, in.
0.065	0.074	-----	-----
.094	-----	0.102	-----
.122	-----	-----	0.130
.638	.192	-----	-----
.667	-----	.220	-----
.695	-----	-----	.248



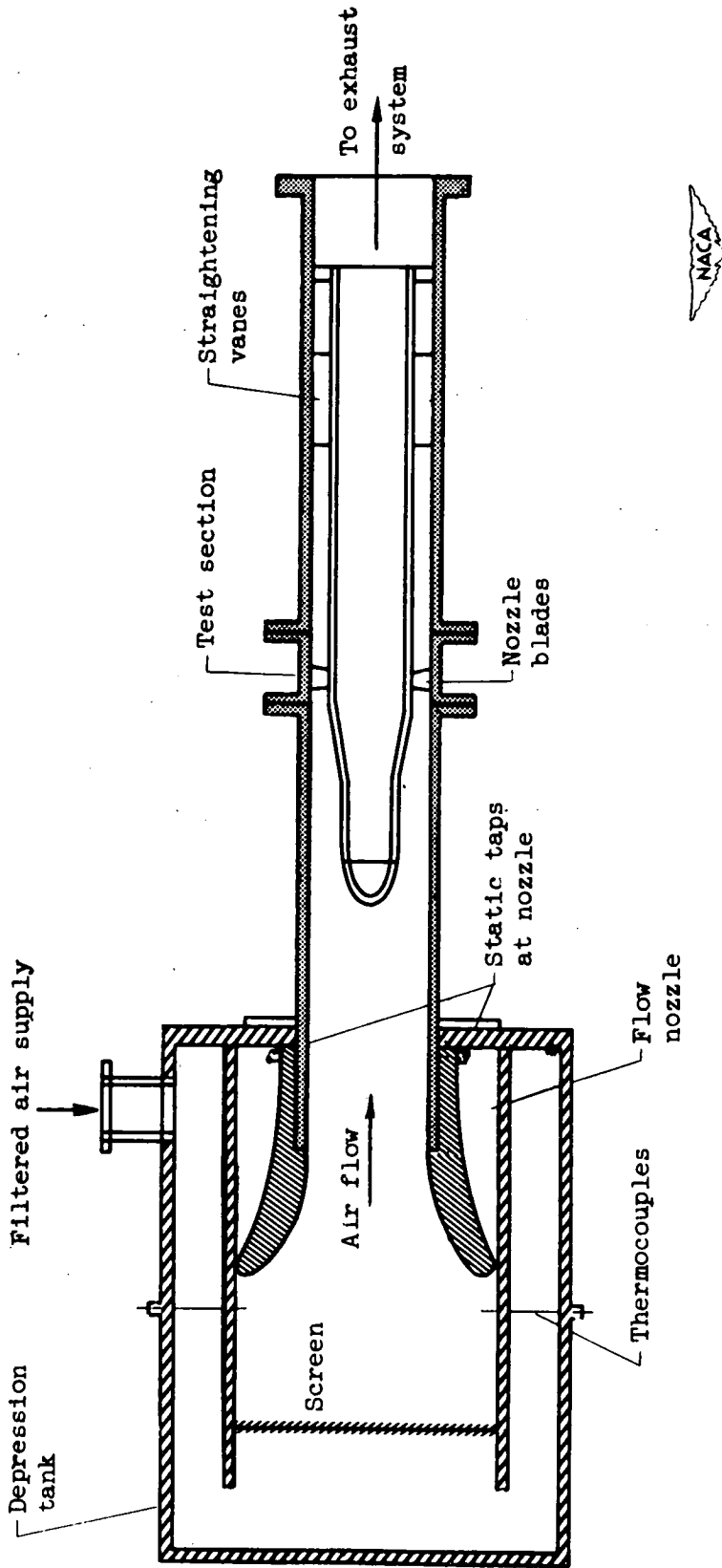
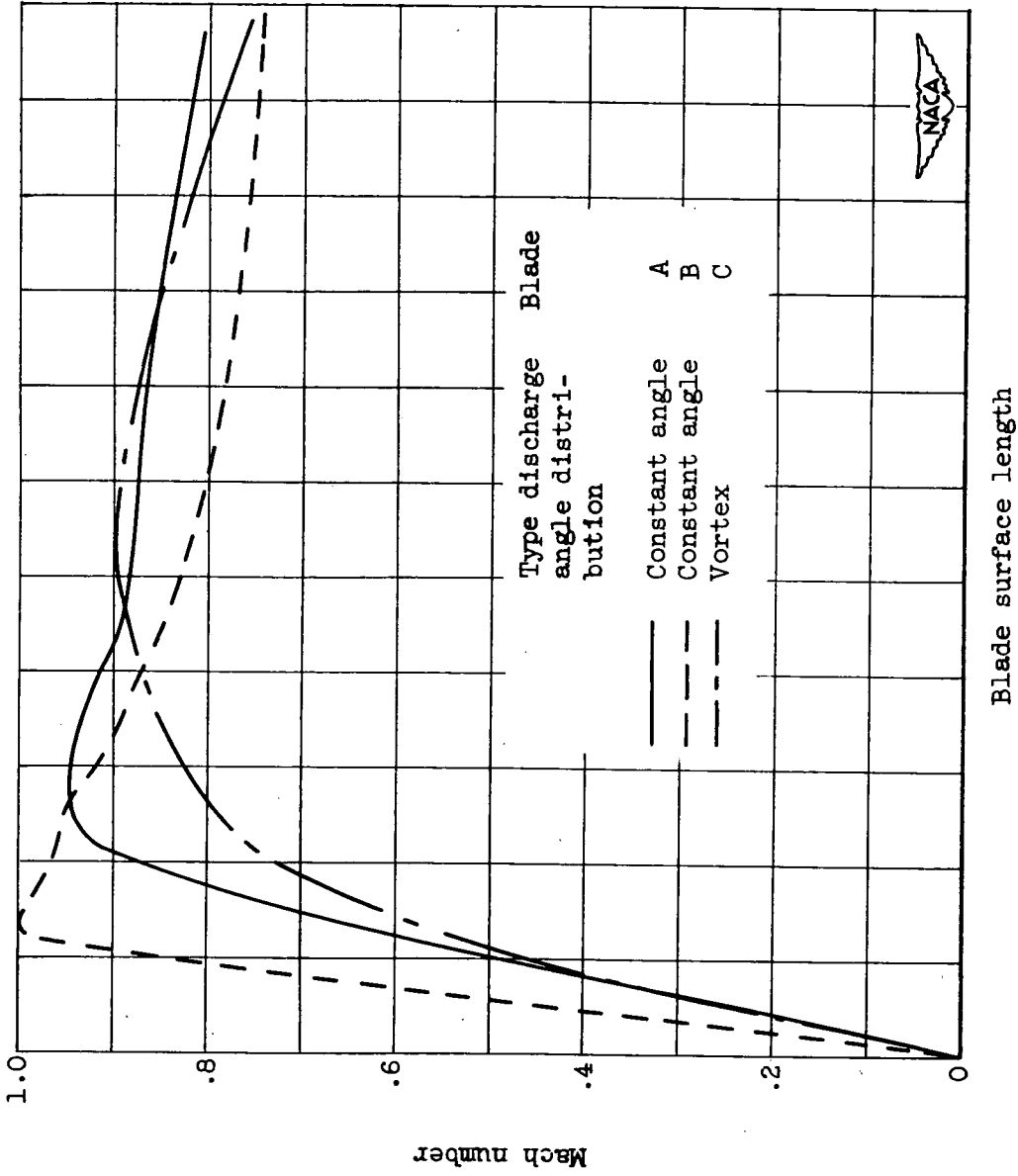
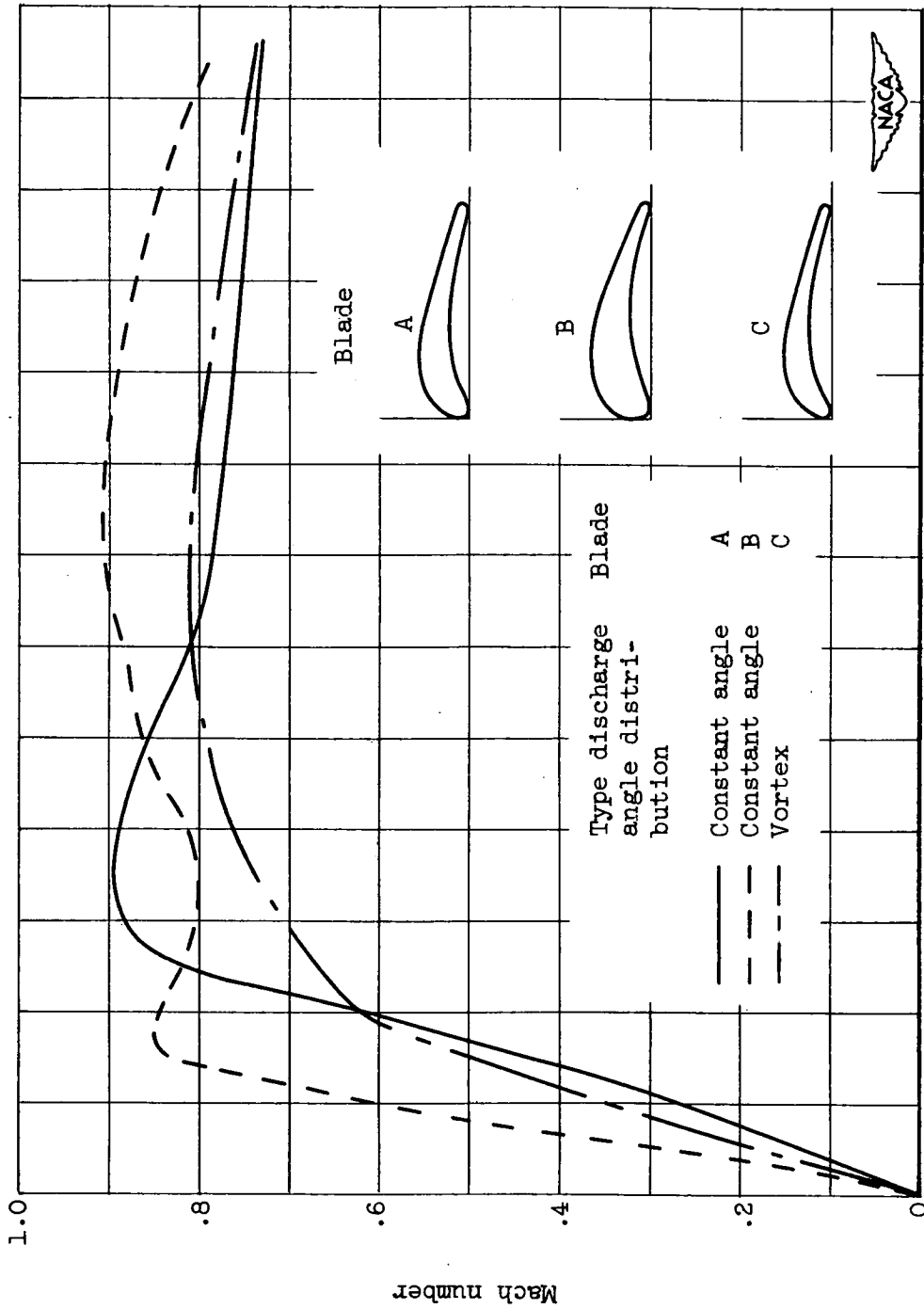


Figure 1. - Schematic view of annular nozzle cascade test unit.



(a) Hub section.

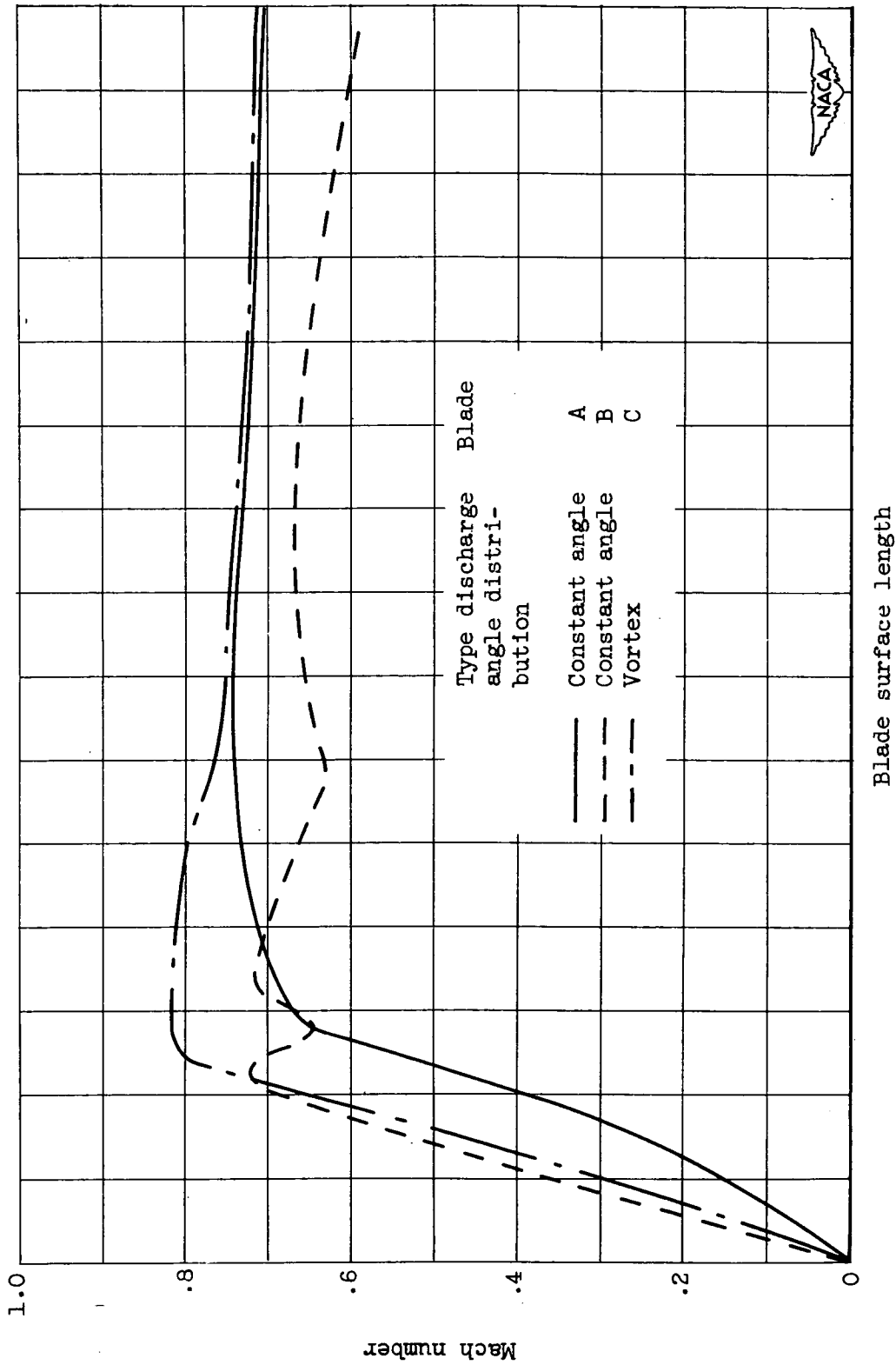
Figure 2. - Design velocities for blade suction surface.



Blade surface length

(b) Mean section.

Figure 2. - Continued. Design velocities for blade suction surface.



(c) Tip section.
 Figure 2. - Concluded. Design velocities for blade suction surface.

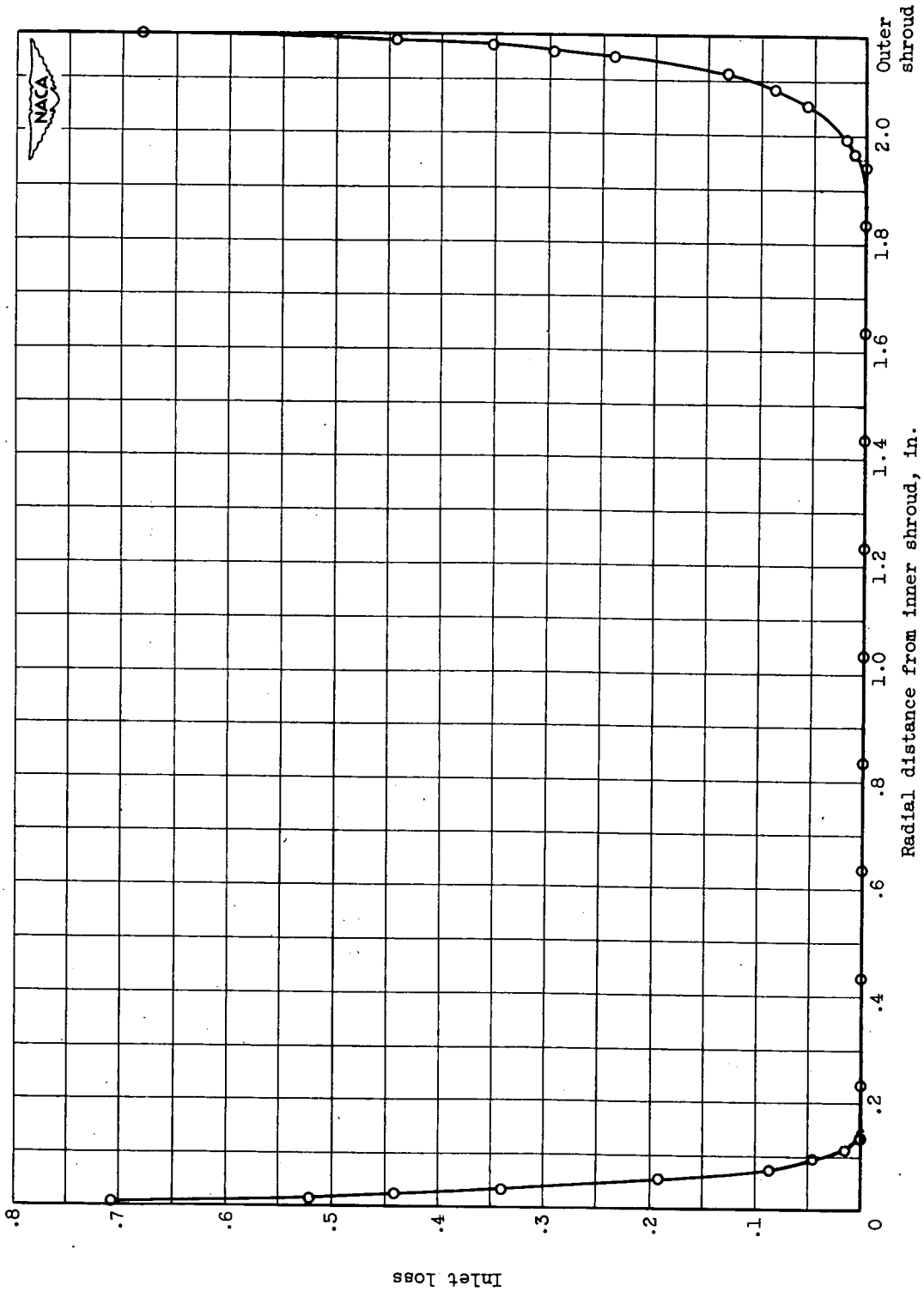
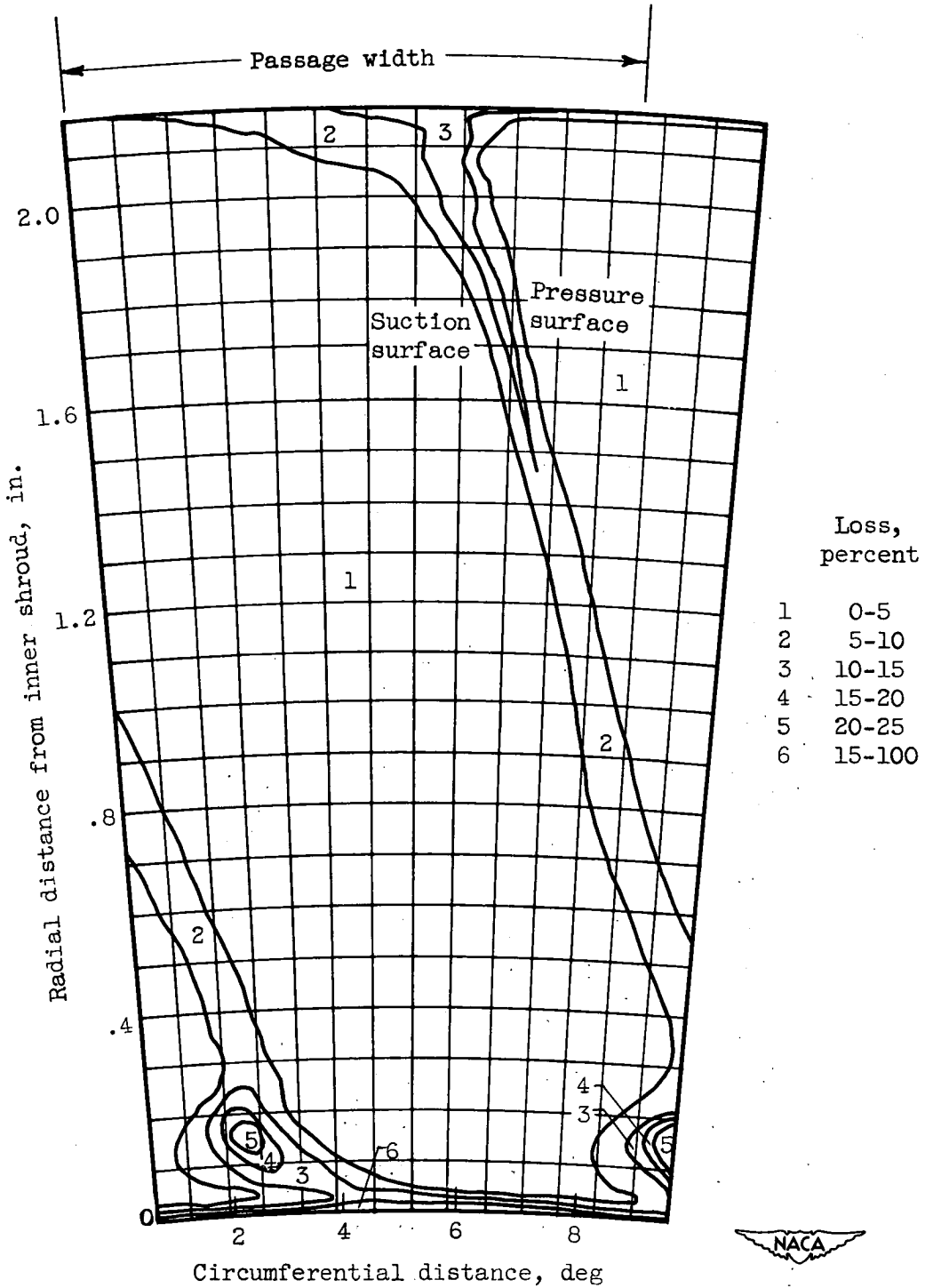
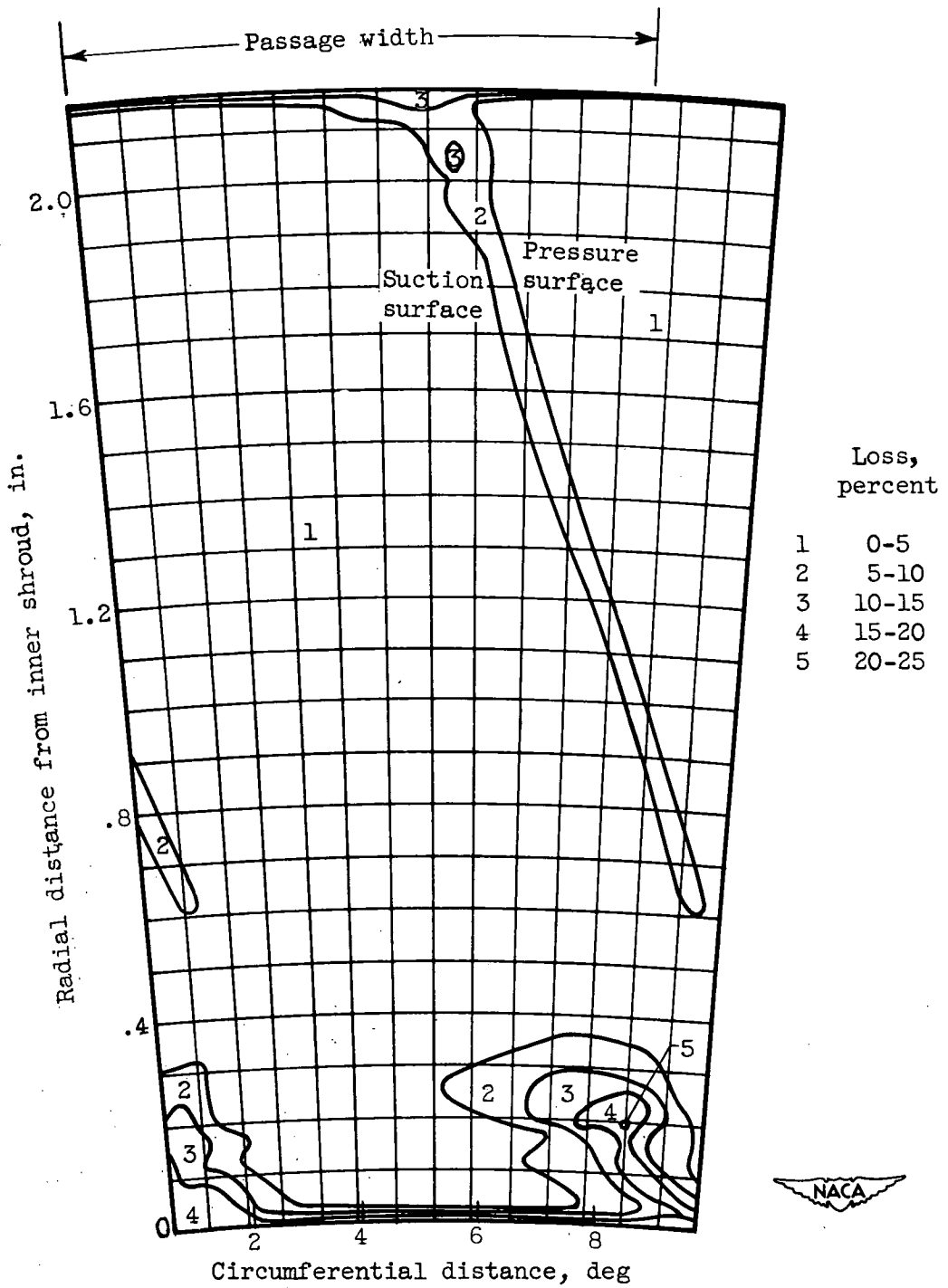


Figure 3. - Radial distribution of inlet loss. Constant-discharge-angle blade A; higher Mach number.



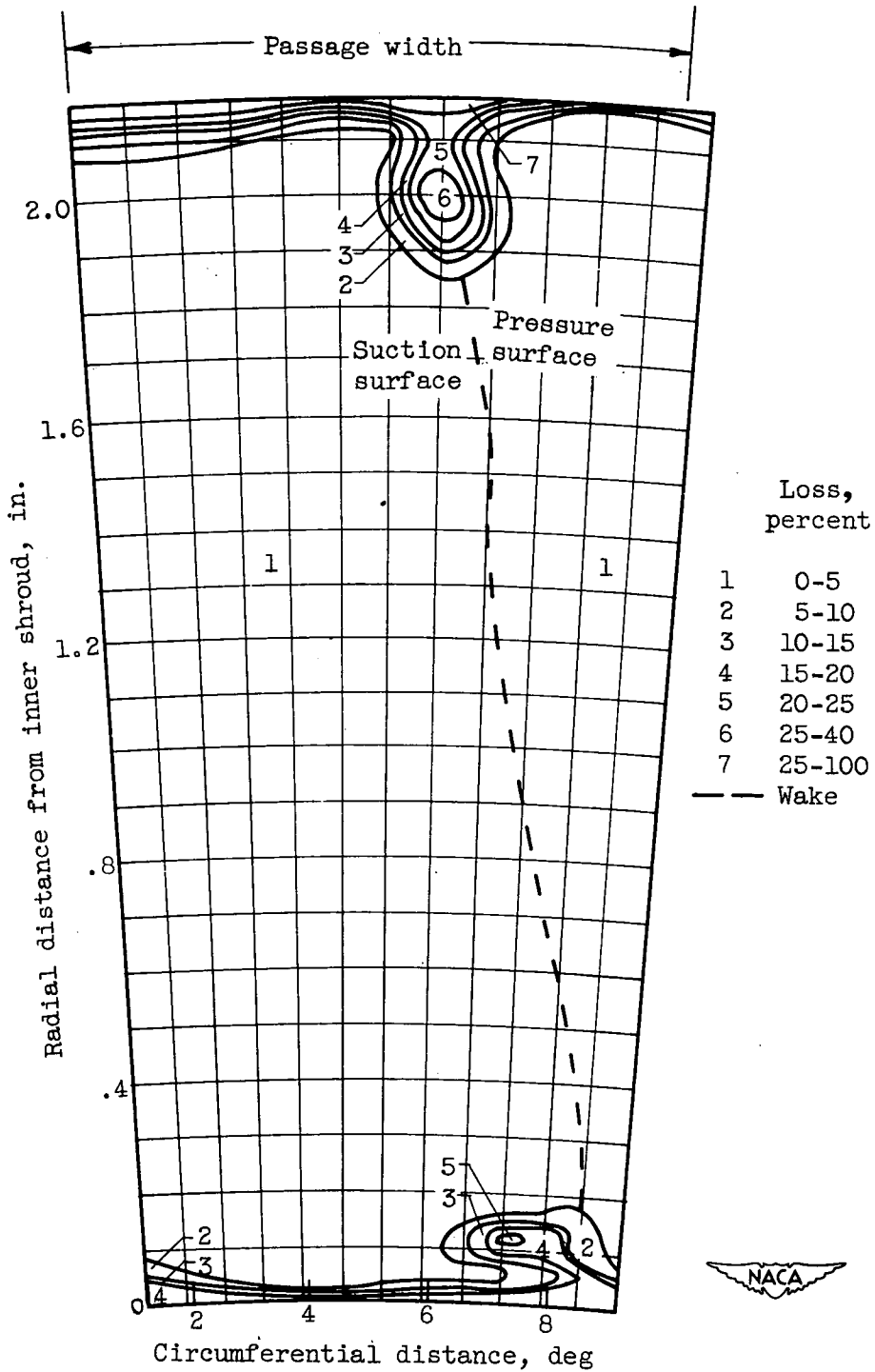
(a) Blade A; lower Mach number ($M_H = 0.86$).

Figure 4. - Contours of loss across one blade passage.



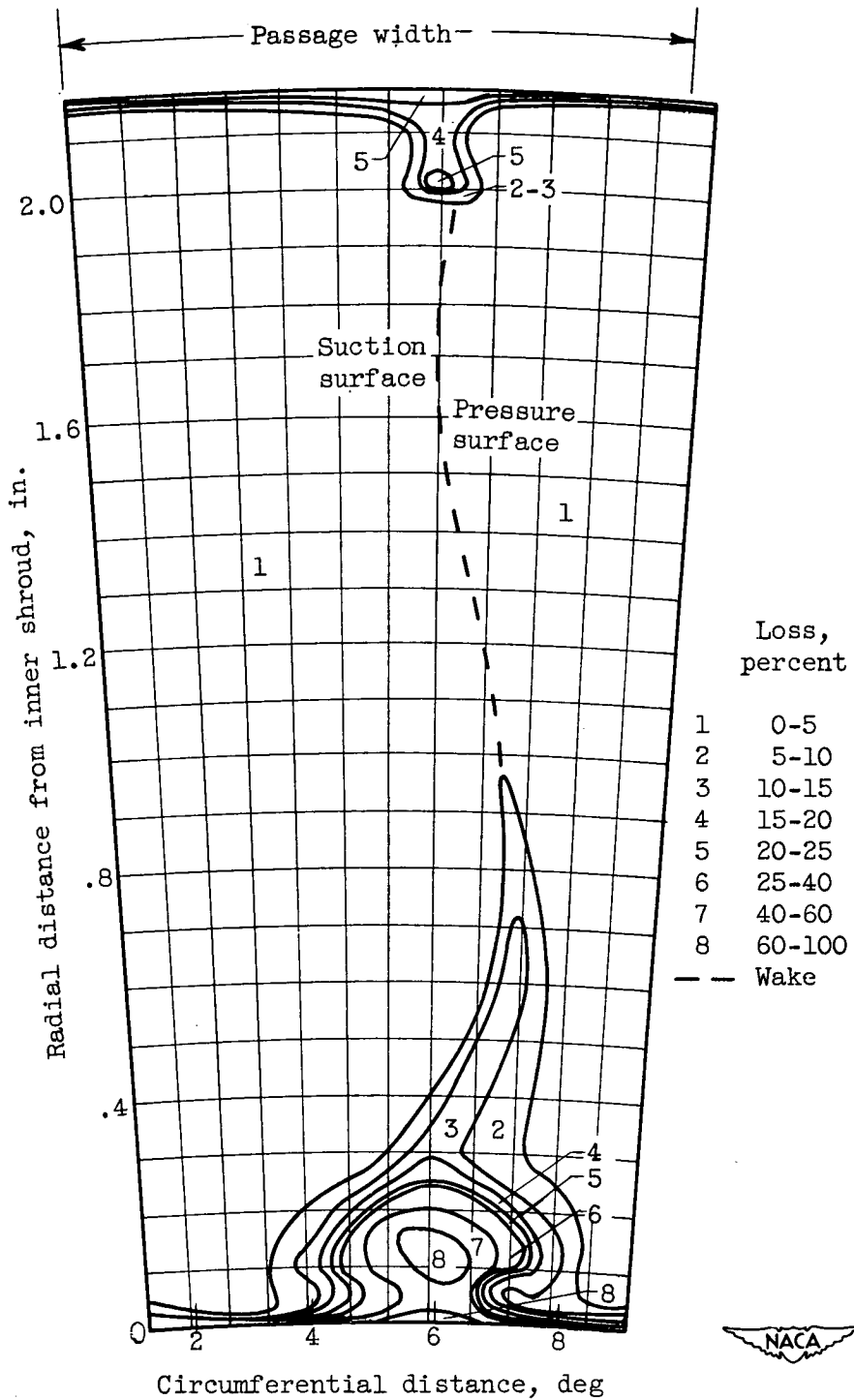
(b) Blade A; higher Mach number ($M_H = 1.36$).

Figure 4. - Continued. Contours of loss across one blade passage.



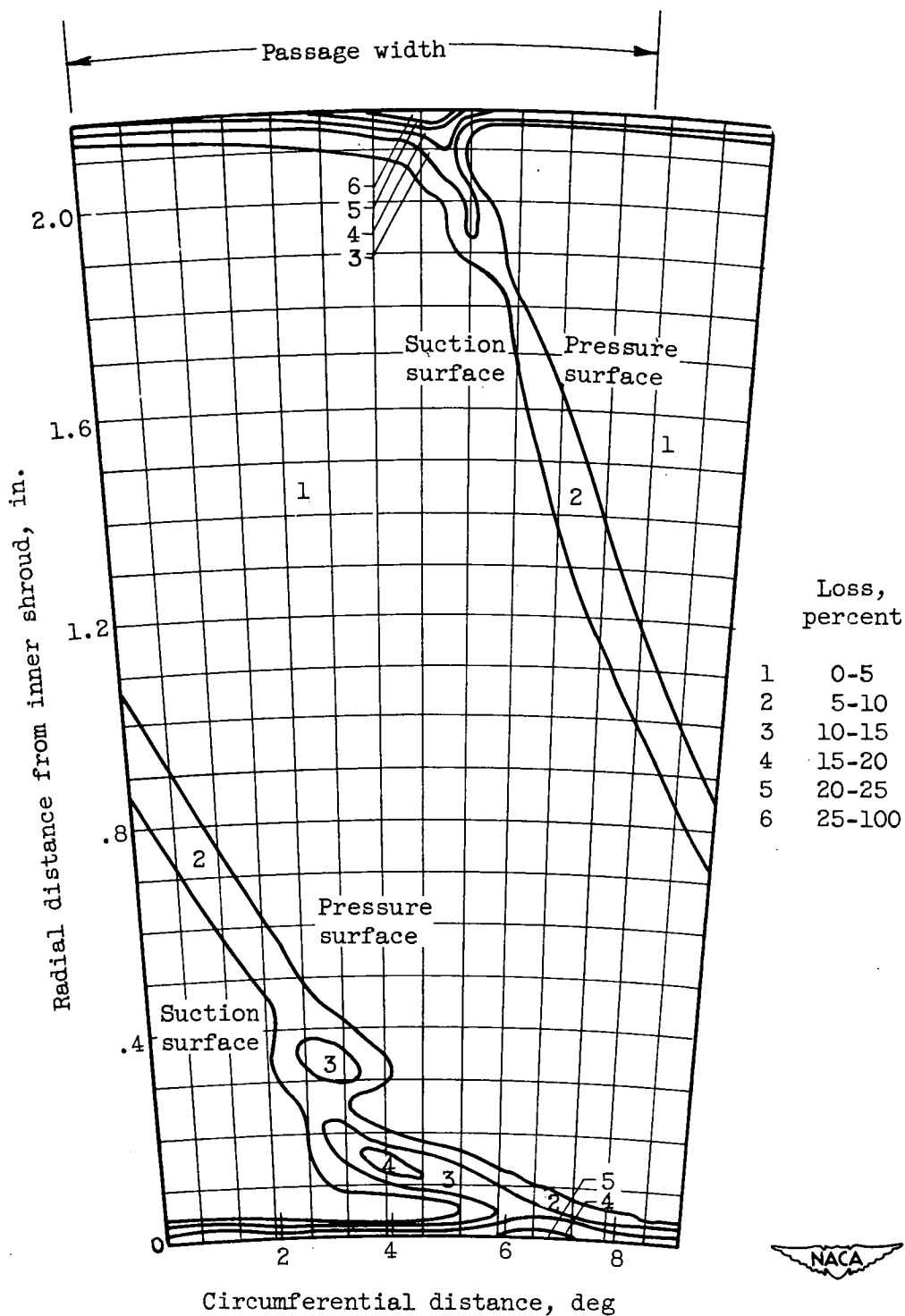
(c) Blade B; lower Mach number ($M_H = 1.18$).

Figure 4. - Continued. Contours of loss across one blade passage.



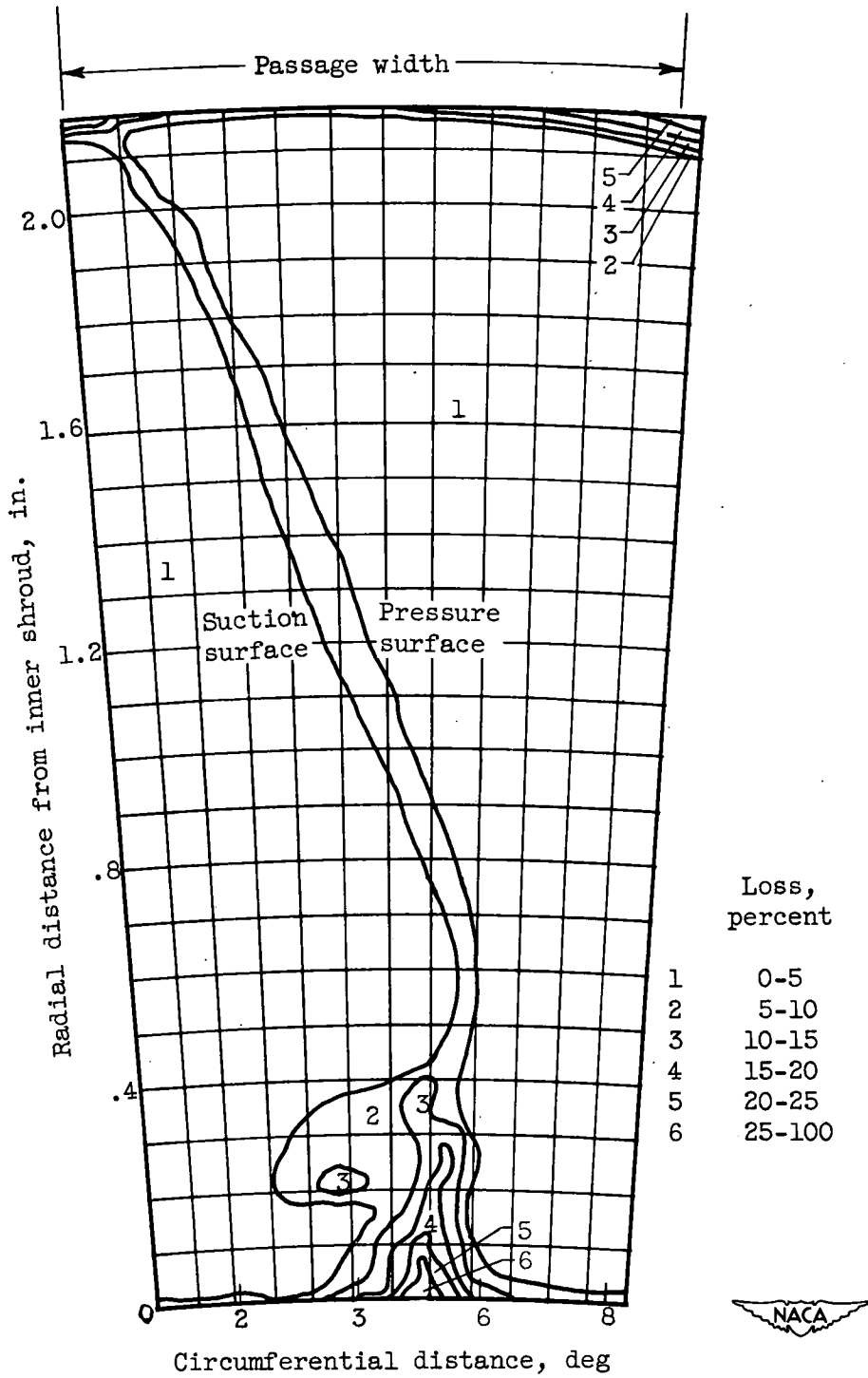
(d) Blade B; higher Mach number ($M_H = 1.41$).

Figure 4. - Continued. Contours of loss across one blade passage.



(e) Blade C; lower Mach number ($M_H = 0.94$).

Figure 4. - Continued. Contours of loss across one blade passage.



(f) Blade C; higher Mach number ($M_H = 1.46$).

Figure 4. - Concluded. Contours of loss across one blade passage.

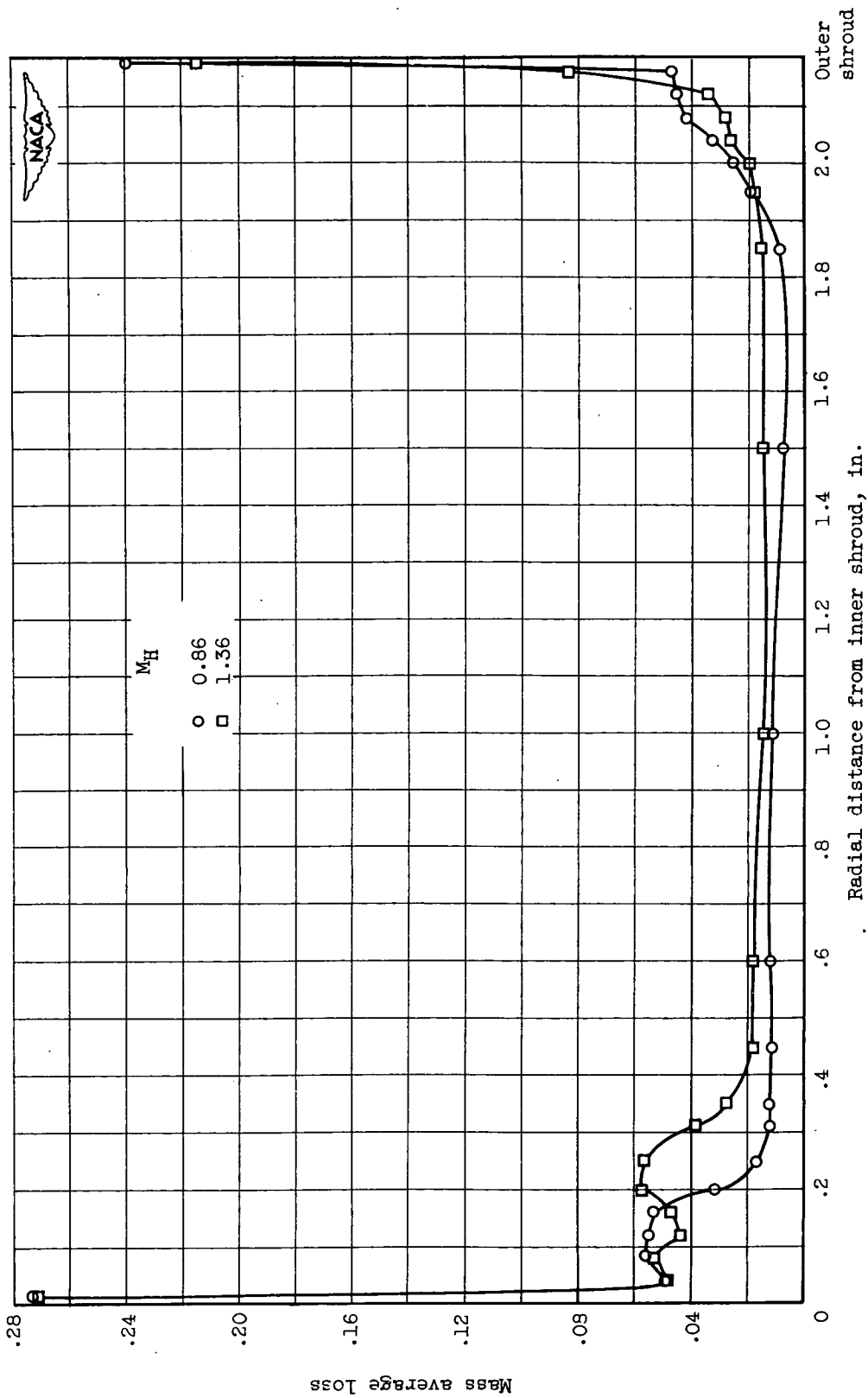
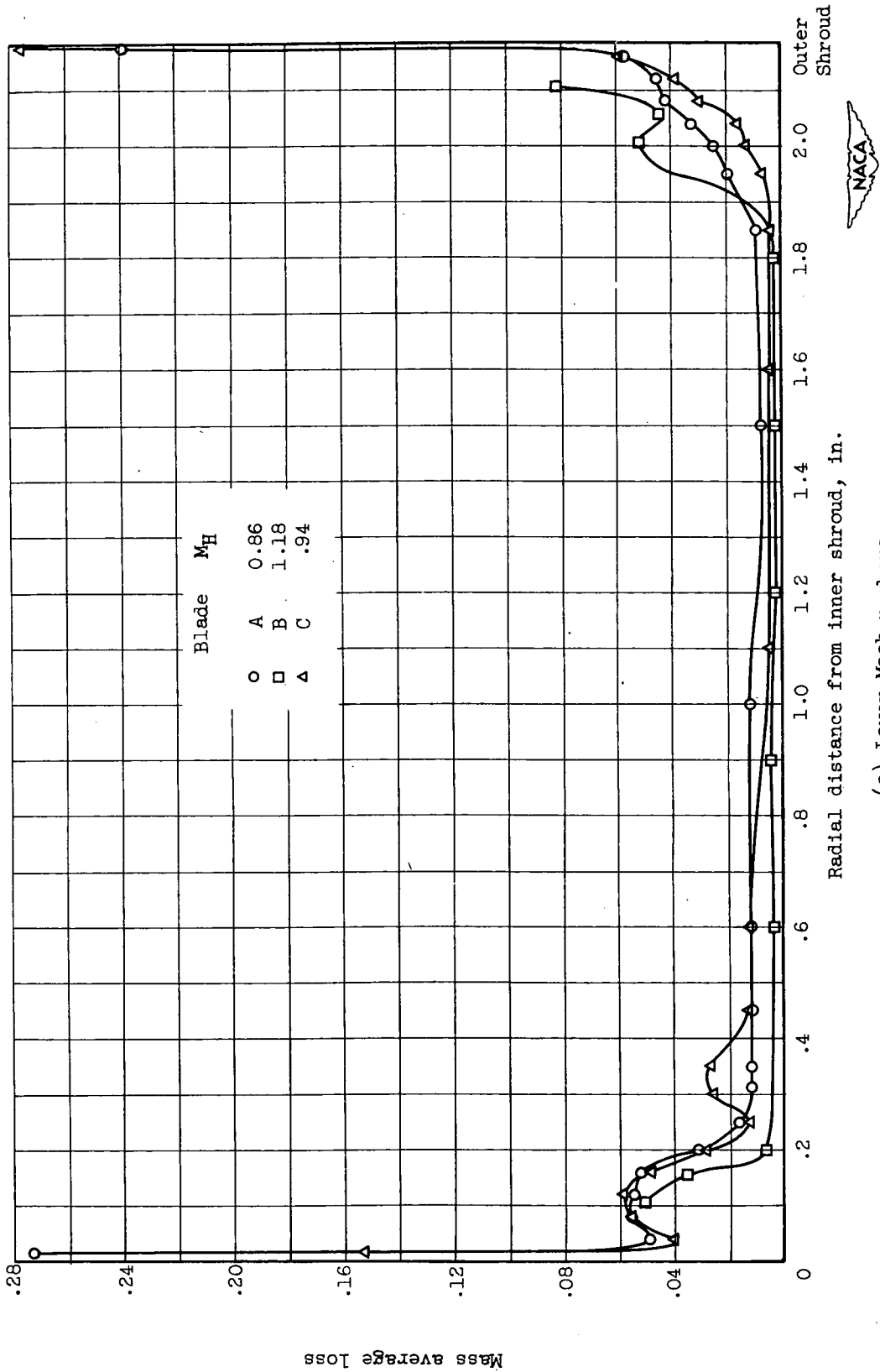


Figure 5. - Radial distribution of loss for blade A.



(a) Lower Mach numbers.

Figure 6. - Comparison of radial distributions of loss.

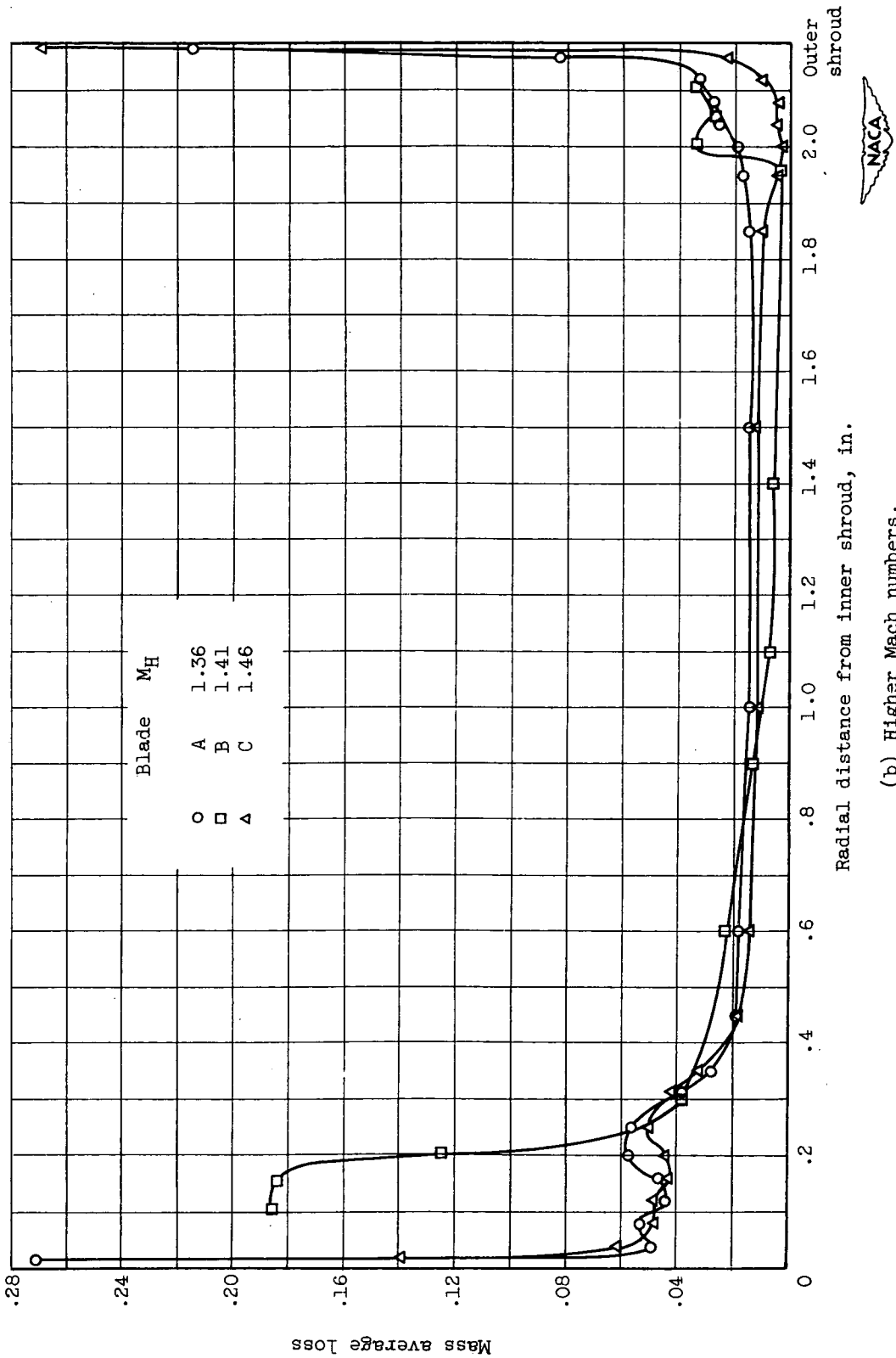
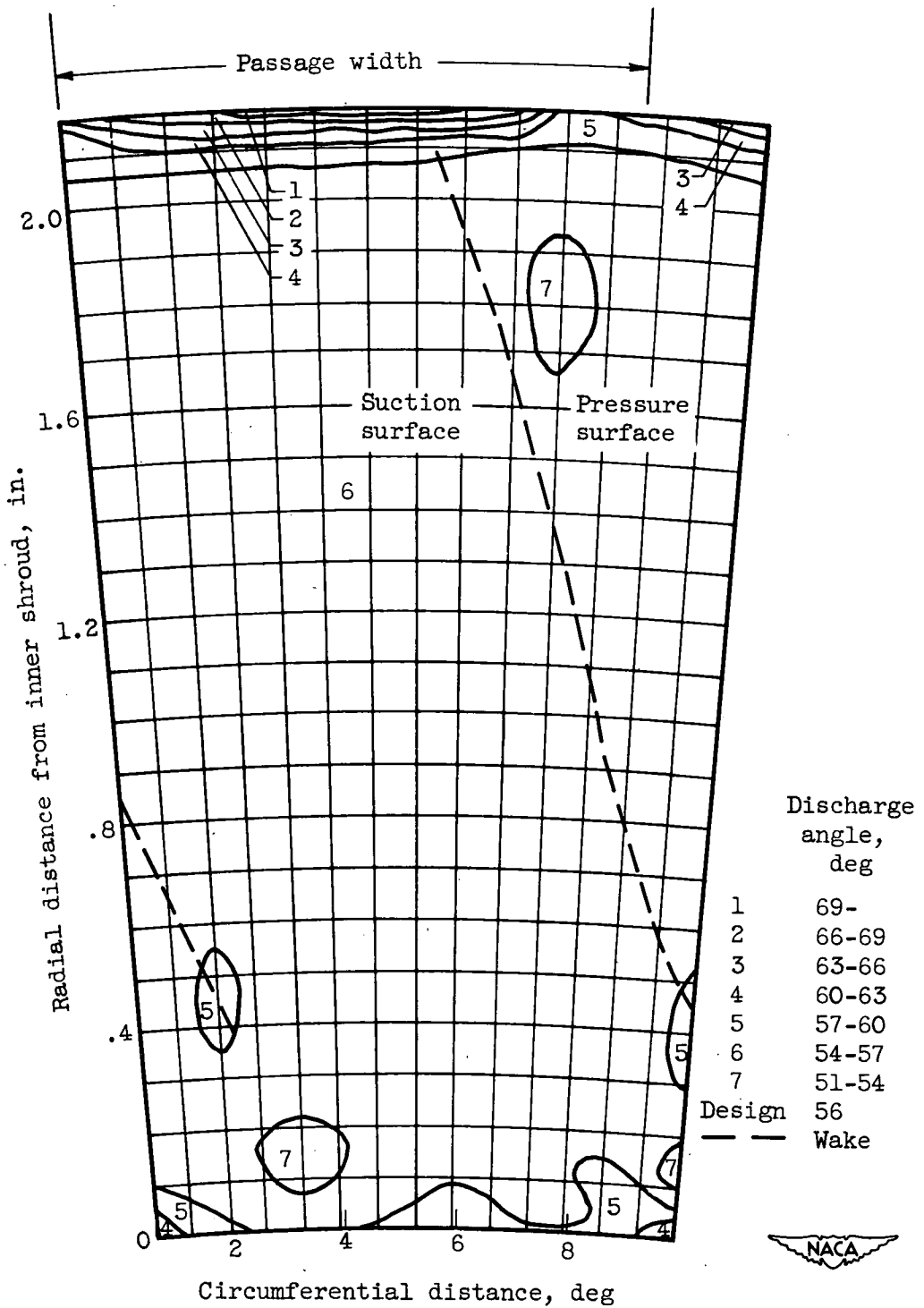


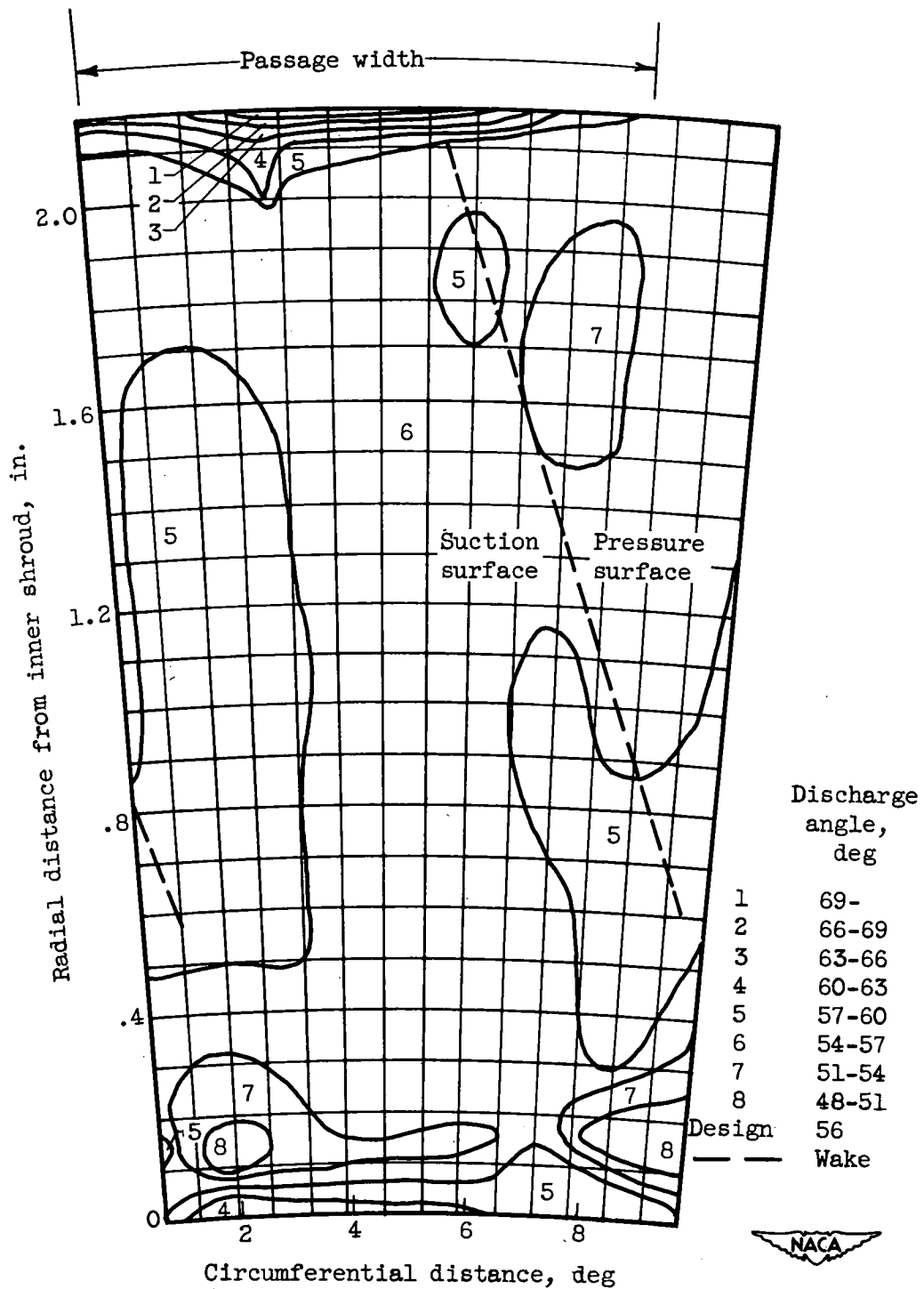
Figure 6. - Concluded. Comparison of radial distributions of loss.

(b) Higher Mach numbers.



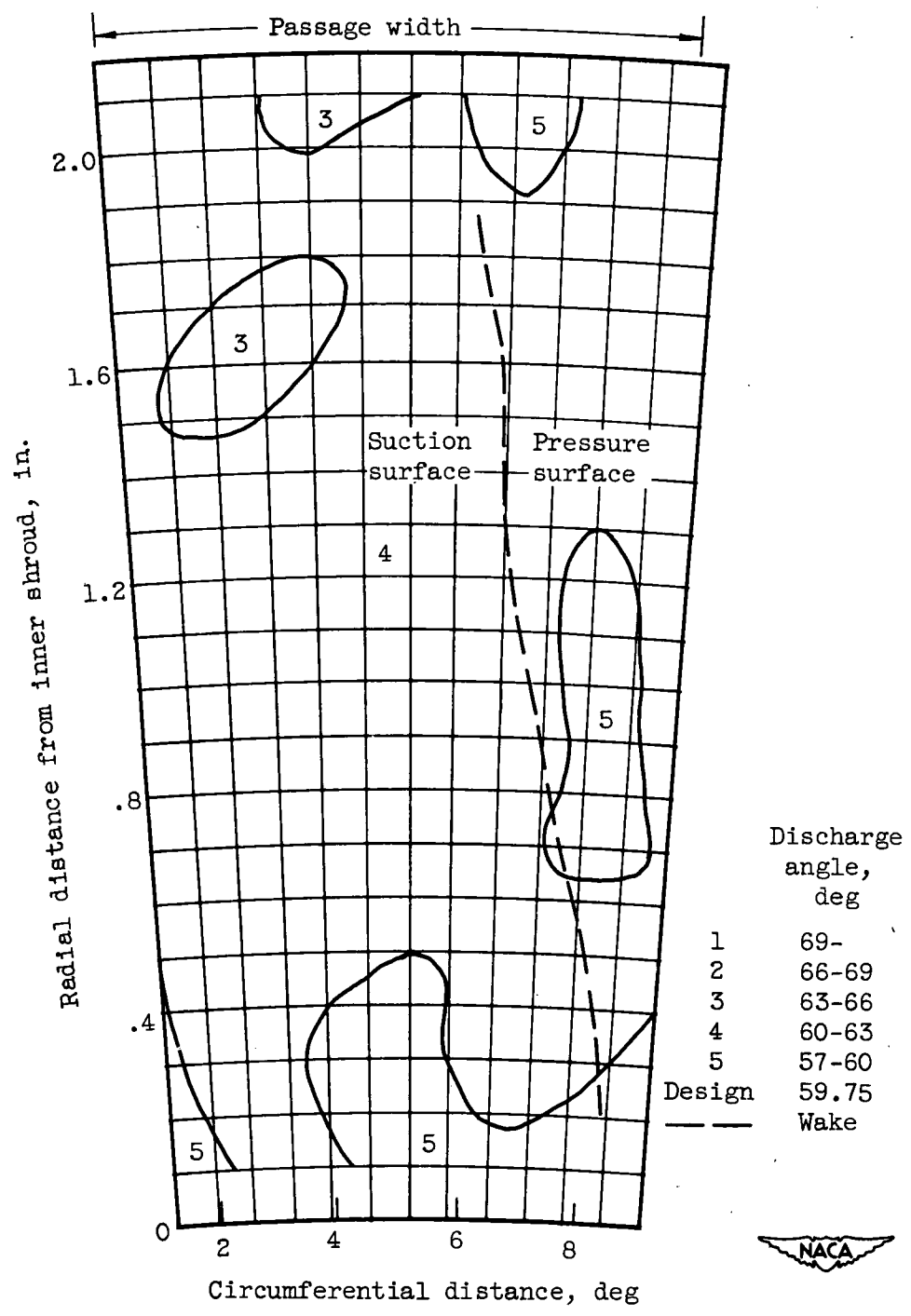
(a) Blade A; lower Mach number ($M_H = 0.86$).

Figure 7. - Contours of discharge flow angle across one blade passage.



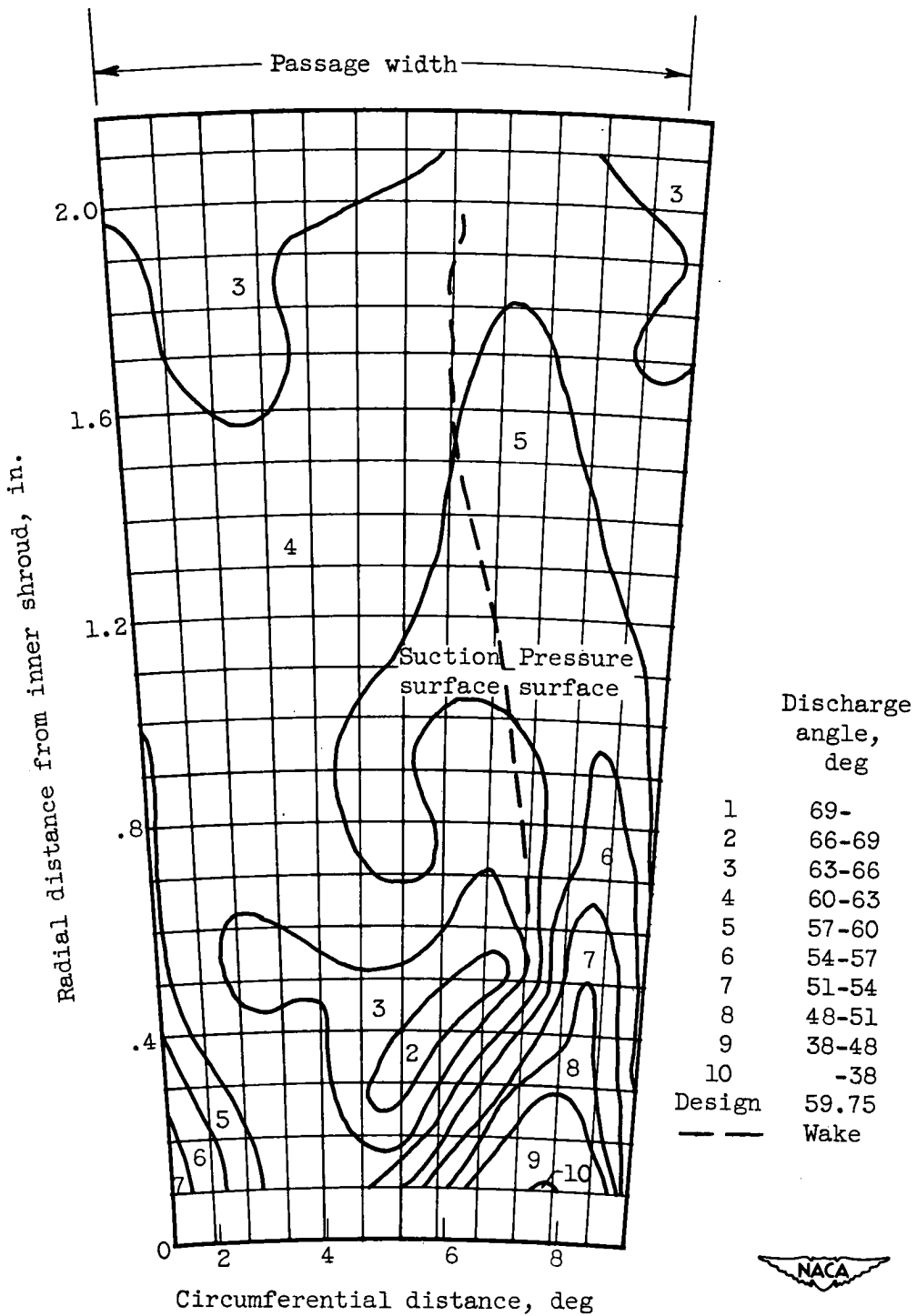
(b) Blade A; higher Mach number ($M_H = 1.36$).

Figure 7. - Continued. Contours of discharge flow angle across one blade passage.



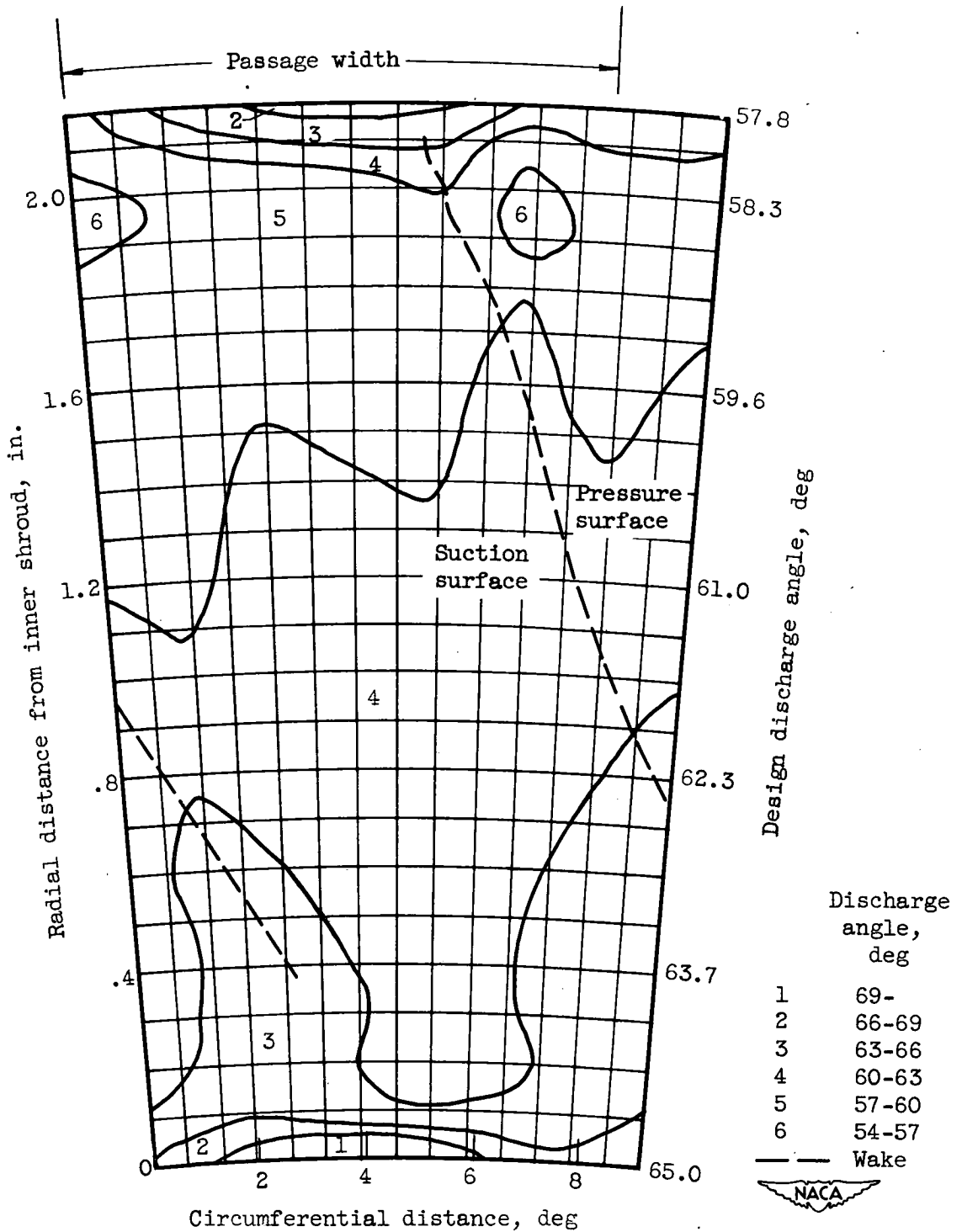
(c) Blade B; lower Mach number ($M_H = 1.18$).

Figure 7. - Continued. Contours of discharge flow angle across one blade passage.



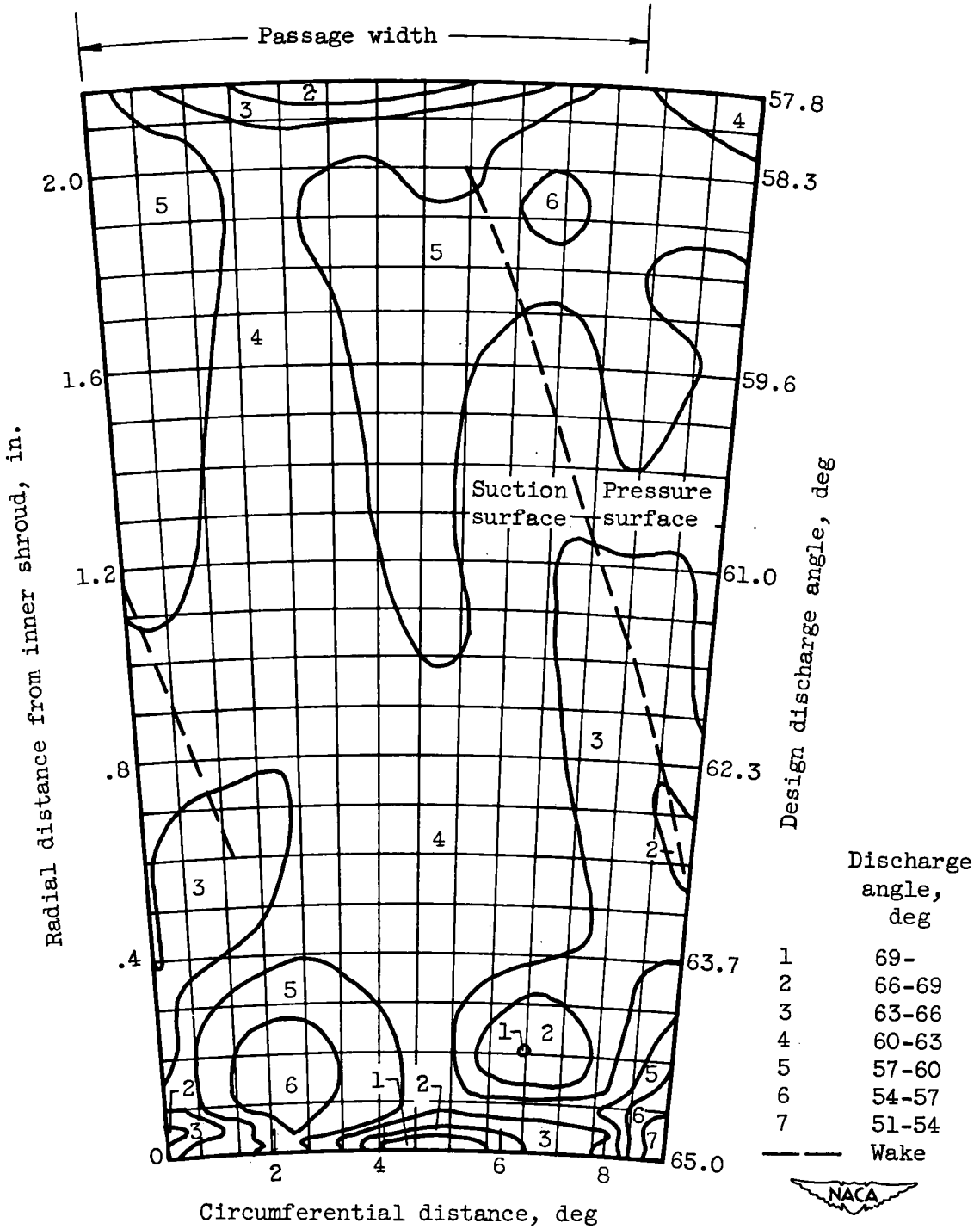
(d) Blade B; higher Mach number ($M_H = 1.41$).

Figure 7. - Continued. Contours of discharge flow angle across one blade passage.



(e) Blade C; lower Mach number ($M_H = 0.94$).

Figure 7. - Continued. Contours of discharge flow angle across one blade passage.



(f) Blade C; higher Mach number ($M_H = 1.46$).

Figure 7. - Concluded. Contours of discharge flow angle across one blade passage.

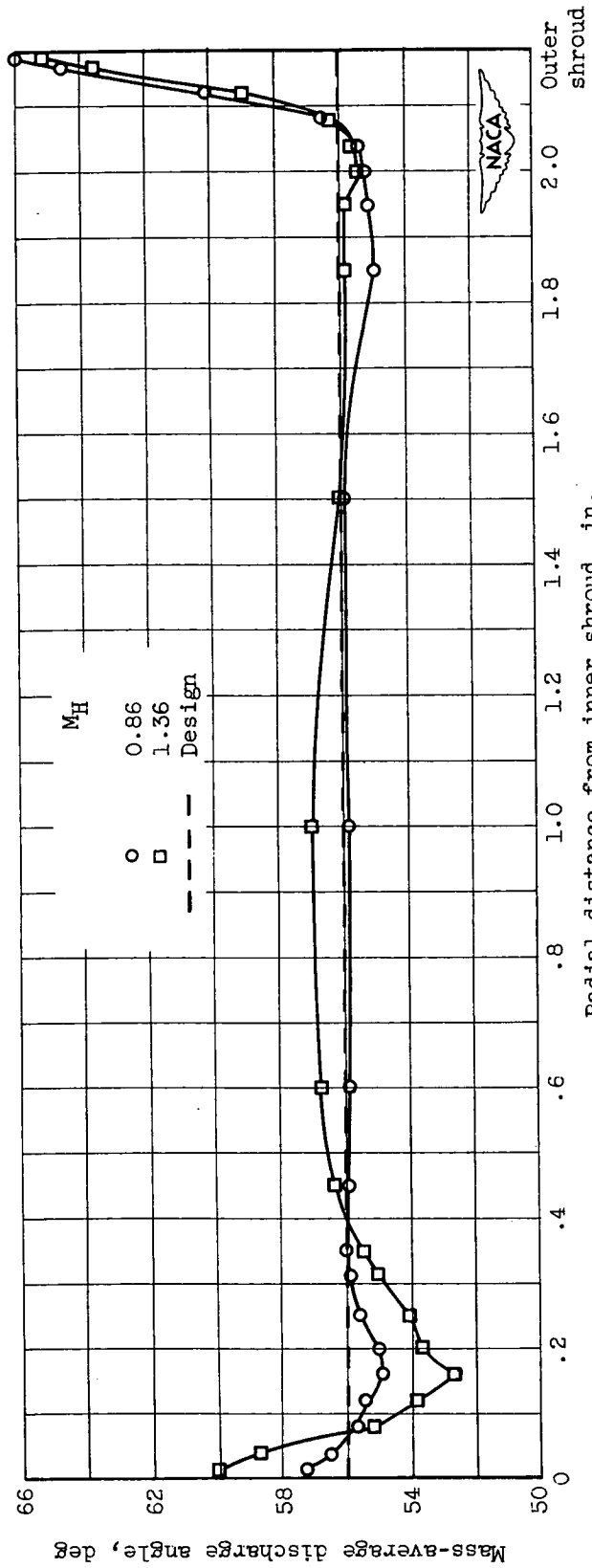
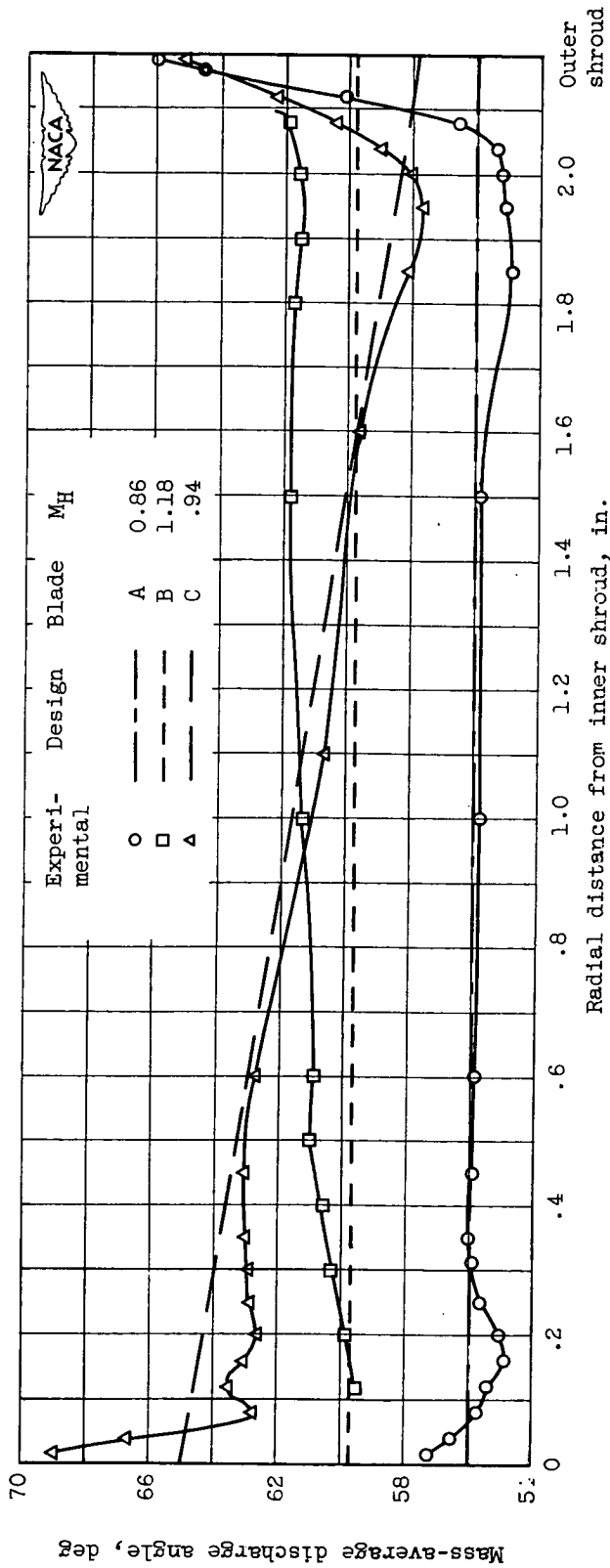
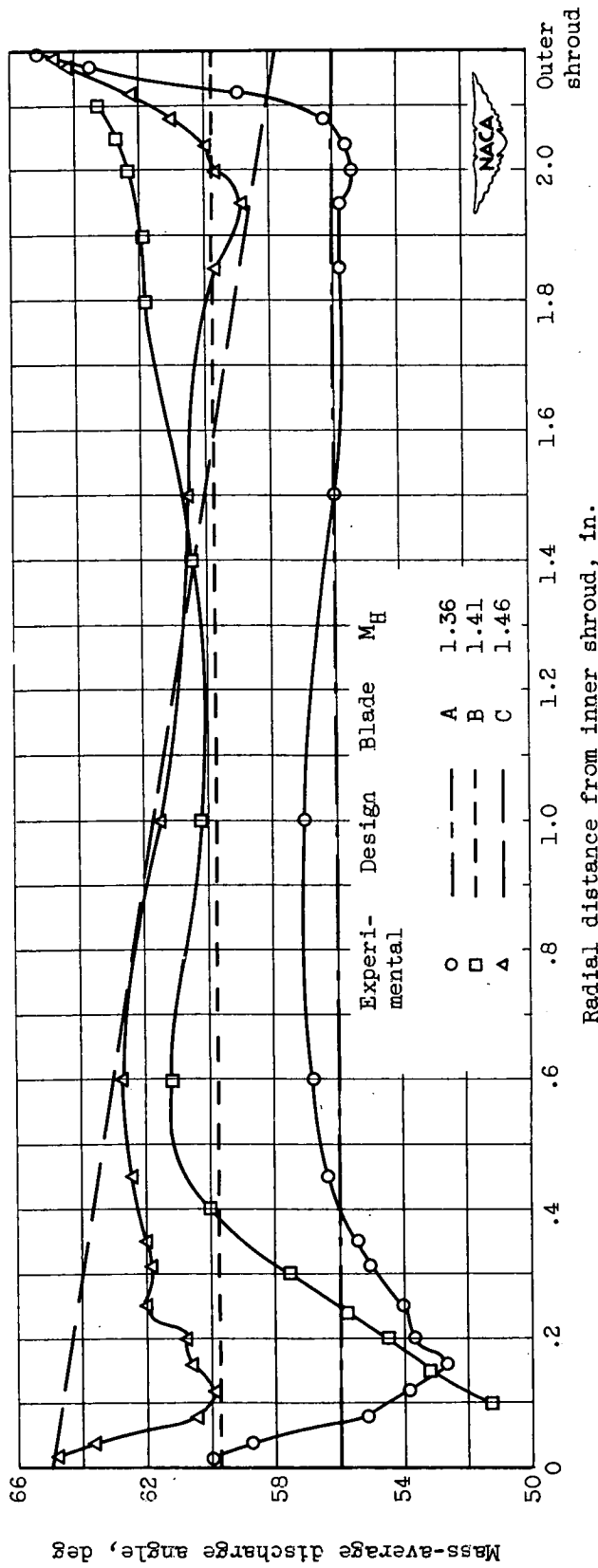


Figure 8. - Radial distribution of discharge angle for blade A.



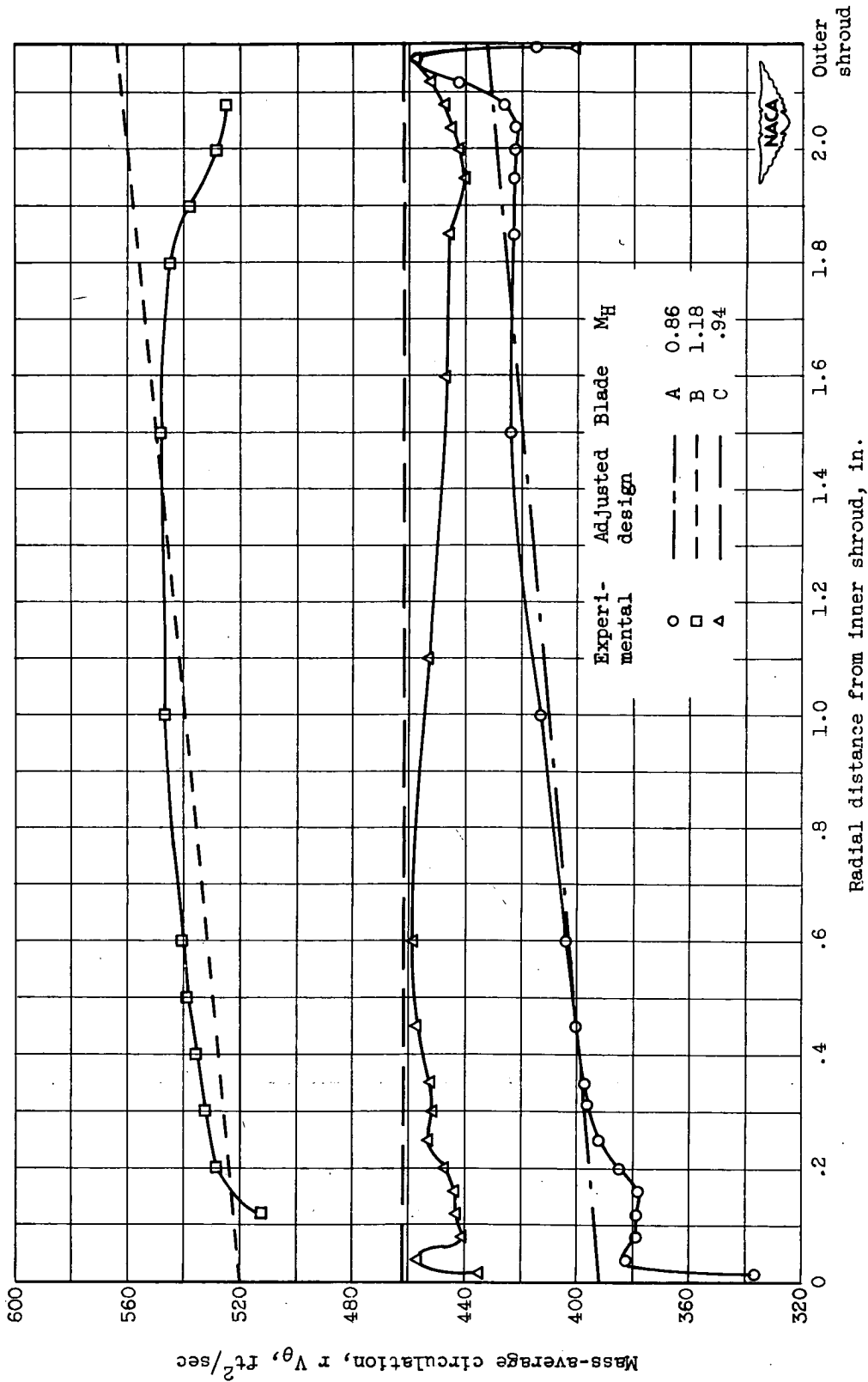
(a) Lower Mach numbers.

Figure 9. - Comparison of radial distributions of discharge angle.



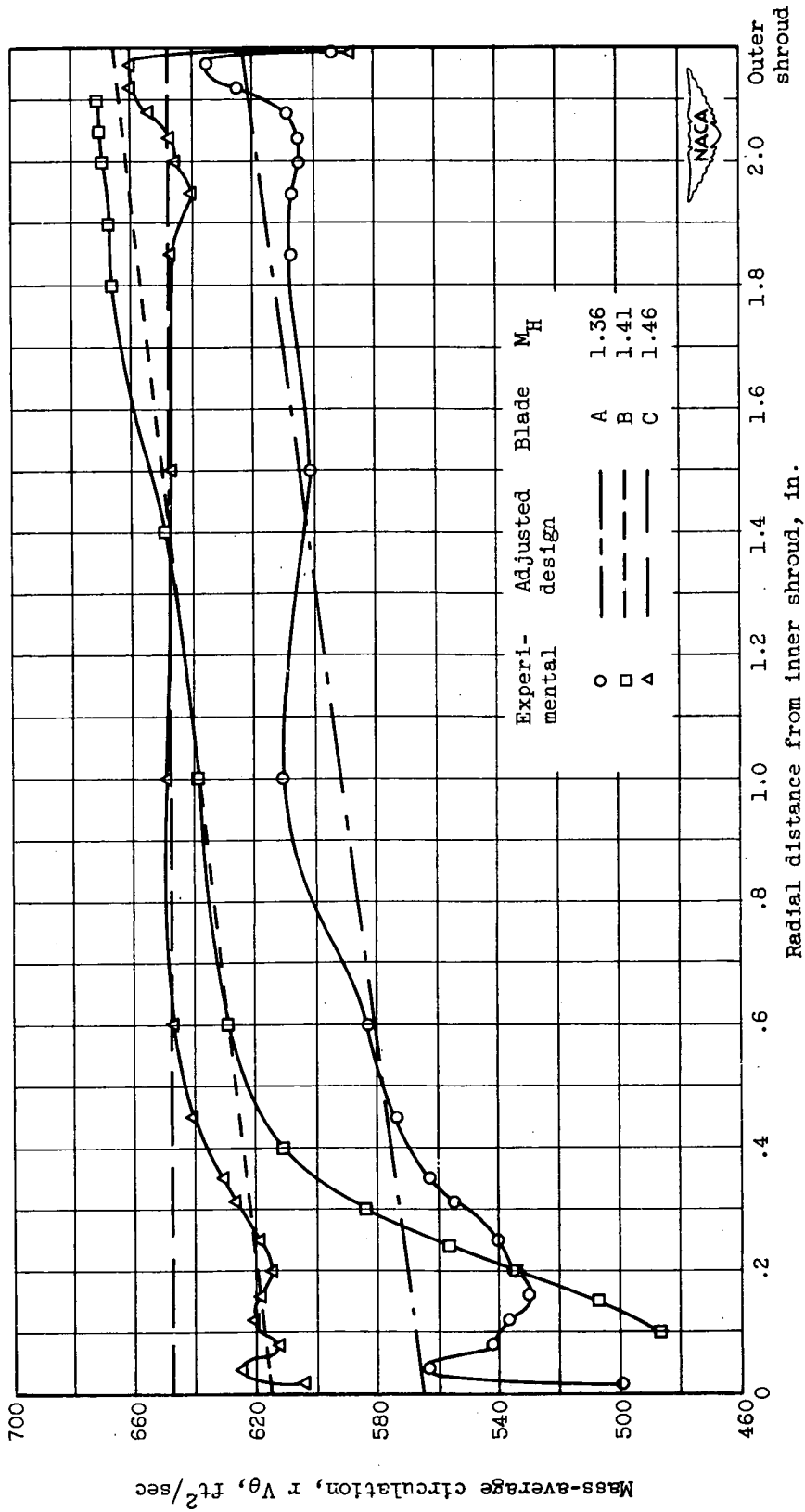
(b) Higher Mach numbers.

Figure 9. - Concluded. Comparison of radial distributions of discharge angle.



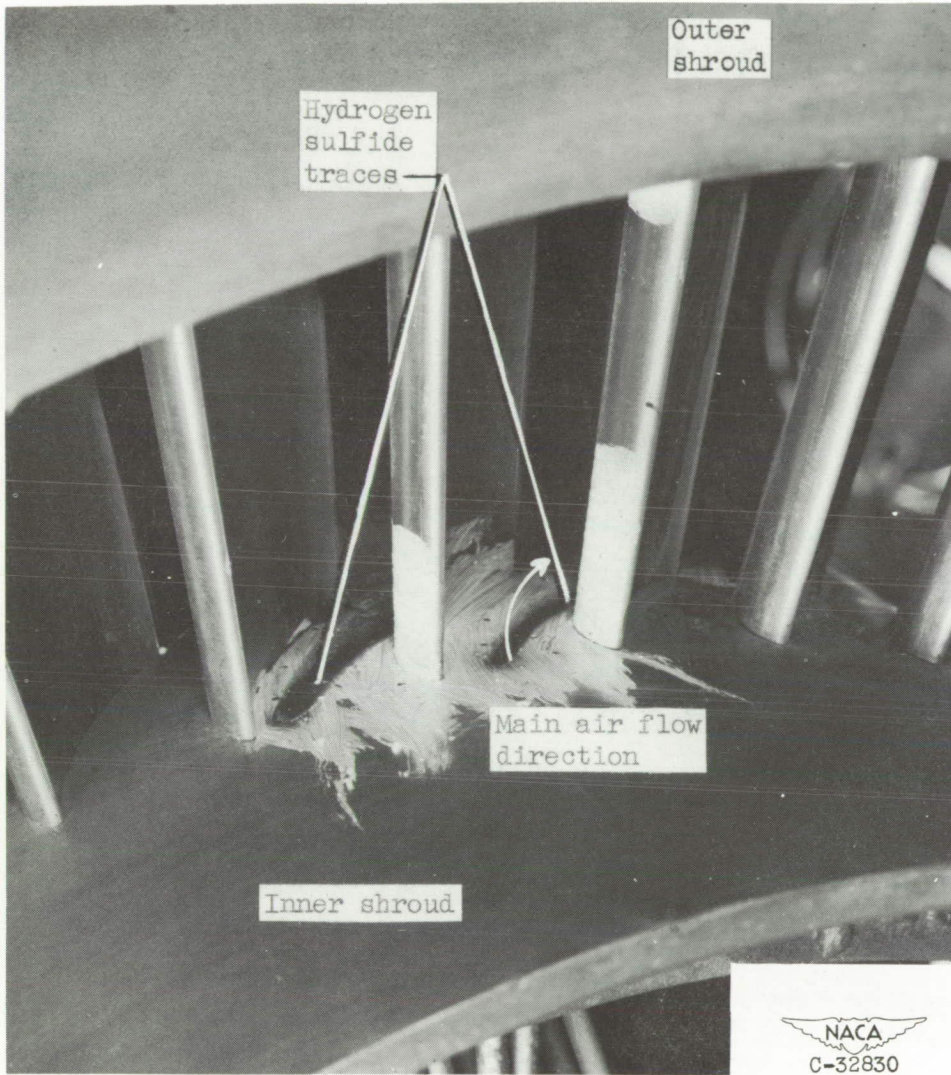
(a) Lower Mach numbers.

Figure 10. - Comparison of radial distributions of circulation.



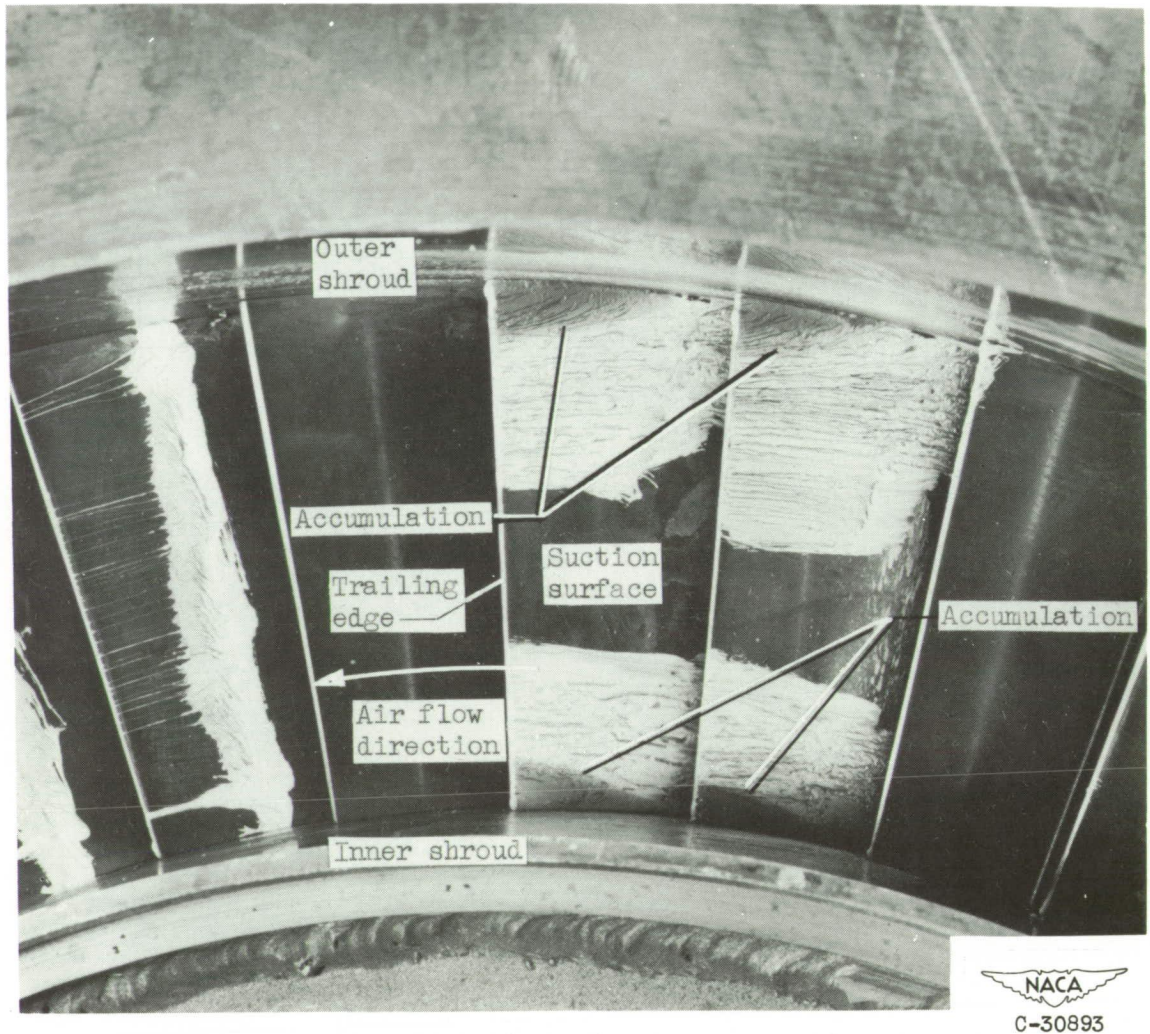
(b) Higher Mach numbers.

Figure 10. - Concluded. Comparison of radial distributions of circulation.



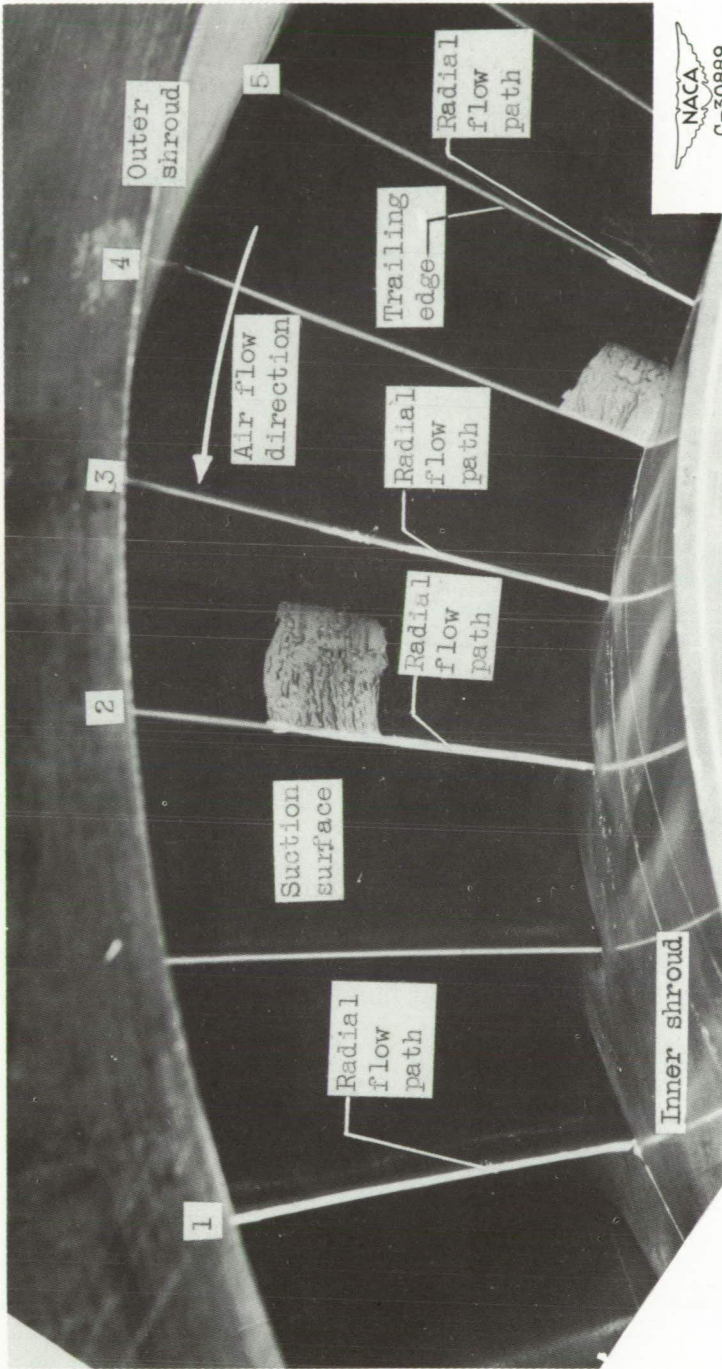
(a) Upstream view of hydrogen sulfide traces.

Figure 11. - Hydrogen sulfide and paint traces at lower Mach number (blade A).



(b) Hydrogen sulfide traces and paint traces at discharge.

Figure 11. - Continued. Hydrogen sulfide and paint traces at lower Mach number (blade A).



(c) Trailing edge paint traces.

Figure 11. - Concluded. Hydrogen sulfide and paint traces at lower Mach number (blade A).

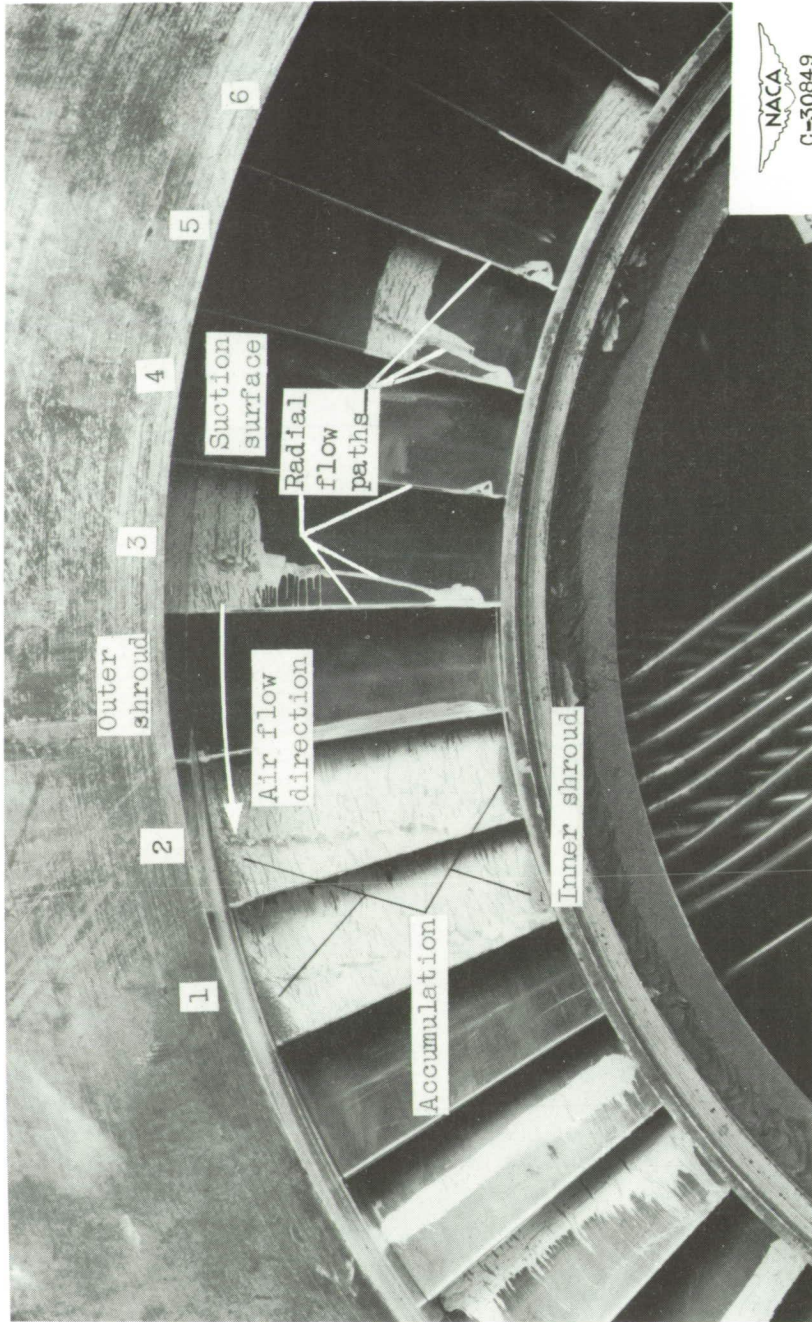
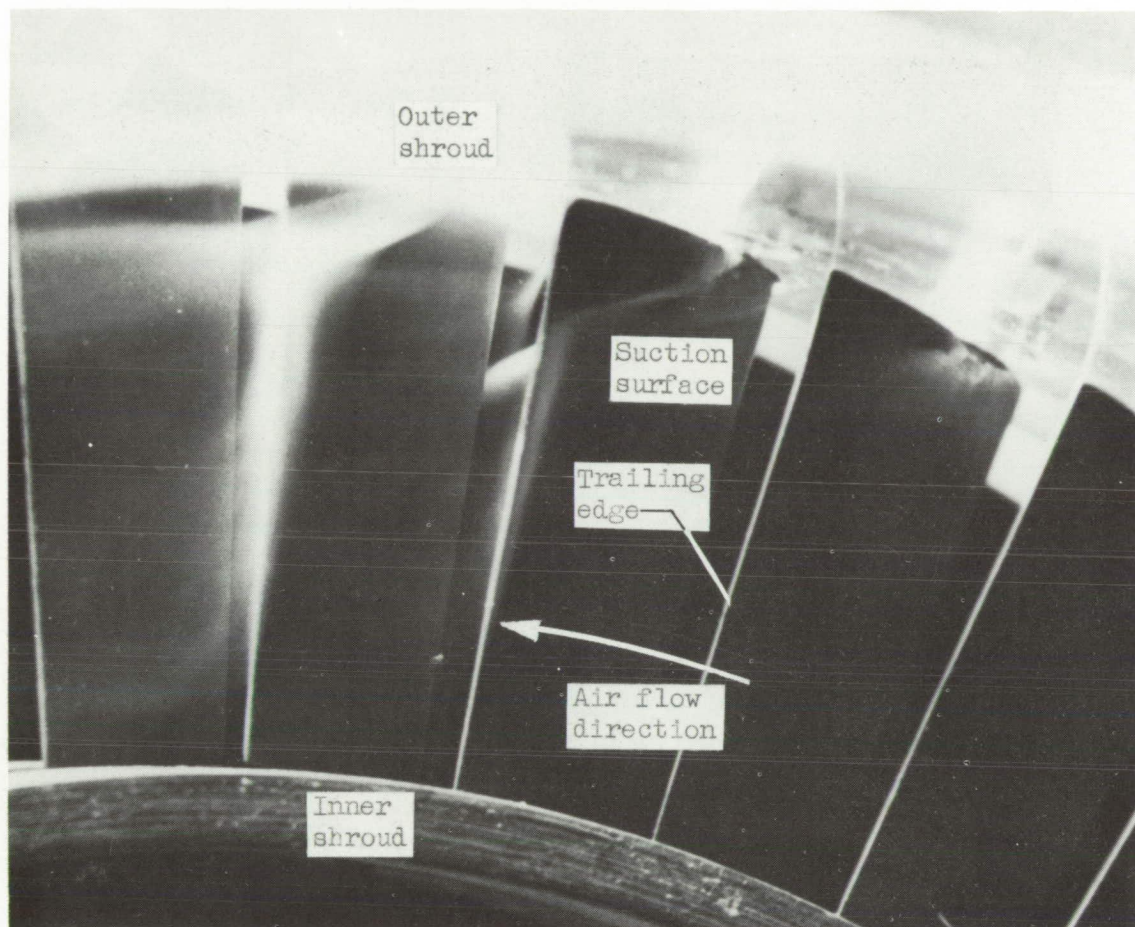
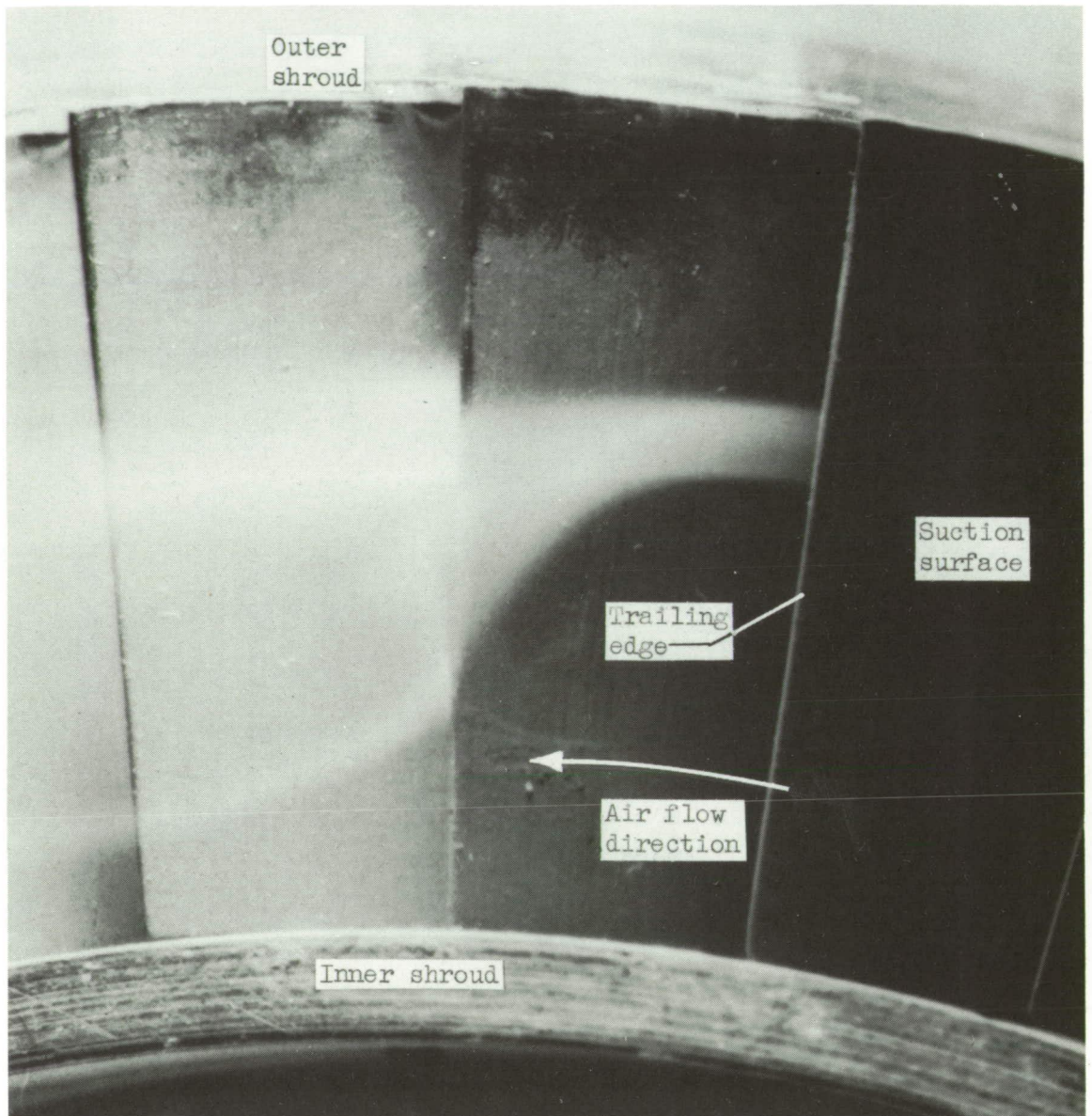


Figure 12. - Hydrogen sulfide traces and paint traces at higher Mach number (blade A).



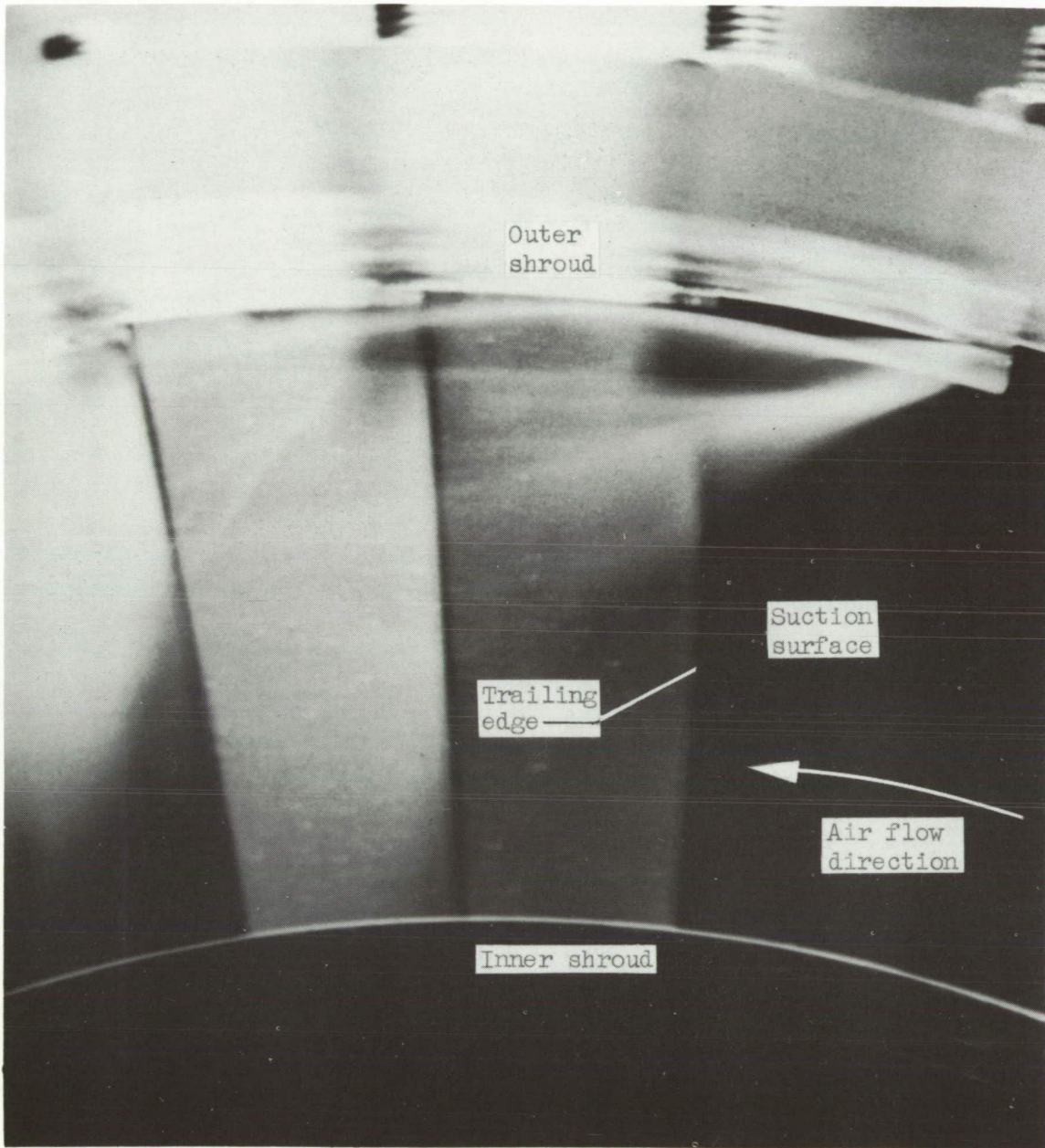
(a) Smoke entering near outer shroud.

Figure 13. - Smoke traces (blade B).



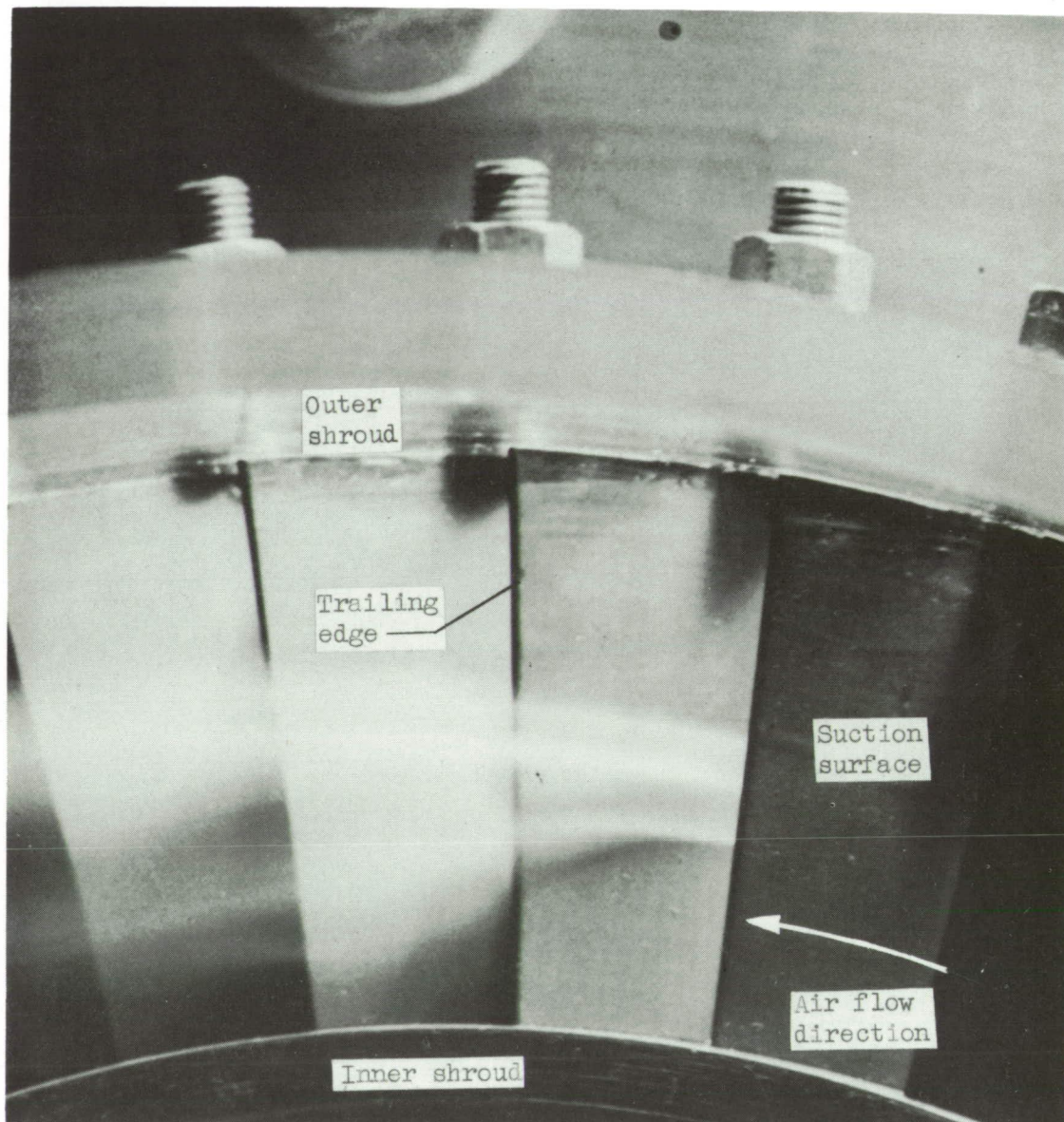
(b) Smoke entering near midspan.

Figure 13. - Concluded. Smoke traces (blade B).



(a) Smoke entering near outer shroud.

Figure 14. - Smoke traces (blade A).



(b) Smoke entering near midspan.

Figure 14. - Concluded. Smoke traces (blade A).

NACA
C-32611